Ultrashort laser pulses and electromagnetic pulse generation in air and on dielectric surfaces

P. Sprangle, J. R. Peñano, B. Hafizi,* and C. A. Kapetanakos†

Naval Research Laboratory, Plasma Physics Division, Washington, DC 20375, USA
(Received 15 August 2003; revised manuscript received 2 March 2004; published 17 June 2004)

Intense, ultrashort laser pulses propagating in the atmosphere have been observed to emit sub-THz electromagnetic pulses (EMPS). The purpose of this paper is to analyze EMP generation from the interaction of ultrashort laser pulses with air and with dielectric surfaces and to determine the efficiency of conversion of laser energy to EMP energy. In our self-consistent model the laser pulse partially ionizes the medium, forms a plasma filament, and through the ponderomotive forces associated with the laser pulse, drives plasma currents which are the source of the EMP. The propagating laser pulse evolves under the influence of diffraction, Kerr focusing, plasma defocusing, and energy depletion due to electron collisions and ionization. Collective effects and recombination processes are also included in the model. The duration of the EMP in air, at a fixed point, is found to be a few hundred femtoseconds, i.e., on the order of the laser pulse duration plus the electron collision time. For steady state laser pulse propagation the flux of EMP energy is nonradiative and axially directed. Radiative EMP energy is present only for nonsteady state or transient laser pulse propagation. The analysis also considers the generation of EMP on the surface of a dielectric on which an ultrashort laser pulse is incident. For typical laser parameters, the power and energy conversion efficiency from laser radiation to EMP radiation in both air and from dielectric surfaces is found to be extremely small, $<10^{-8}$. Results of full-scale, self-consistent, numerical simulations of atmospheric and dielectric surface EMP generation are presented. A recent experiment on atmospheric EMP generation is also simulated.

I. INTRODUCTION

Propagation of intense, ultrashort laser pulses in the atmosphere has demonstrated a wide range of phenomena that may have a variety of applications. The observations include formation and stable, long-distance propagation of optical and plasma filaments, "white" light generation, and emission of sub-THz electromagnetic pulses [1–18]. Terahertz radiation has a wide range of applications in areas such as chemical identification, biomedical diagnostics, and dielectric measurements. In addition, tomographic imaging using THz radiation has potential applications in biomedical research, security screening, and remote sensing. Terahertz radiation is also generated by backward wave oscillators [19], gyrotrons [20], free-electron lasers [21], difference-frequency mixing in nonlinear media [22], photoconductive switches [23], tunable optical parametric oscillators [24], semiconductor lasers [25], optically pumped THz lasers [26], dc to ac converters [27], and Cherenkov wakes in magnetized plasmas [28].

Recently, it has been observed that a broadband electromagnetic pulse (EMP) of terahertz radiation can be generated within the plasma filaments formed by an ultrashort ($\sim$100 fsec), high-intensity ($\sim10^{13}$–10^{14} W/cm^2) laser pulse propagating in air [14,17]. In these experiments the laser pulse was sufficiently intense to create a plasma filament through multiphoton ionization of air. The plasma density within the filament was observed to be $\sim10^{16}$ cm^{-3}. This

density corresponds to a plasma wavelength of $\sim$330 μm and a plasma frequency of $\sim$0.9 THz.

In this paper we analyze and numerically simulate the EMP produced by the interaction of ultrashort laser pulses with air and dielectric surfaces, and determine the conversion efficiency from the laser pulse energy to EMP. Atmospheric EMP is generated when a short, intense laser pulse ionizes the air and forms a plasma filament. The plasma filament extends behind and its front travels with the laser pulse as indicated in Fig. 1. The duration of the plasma current which drives the EMP is limited by the electron collision frequency. For a plasma density of $n_e \sim 10^{16}$ cm^{-3}, the electron collision frequency is $\nu_e \sim 5\times10^{12}$ sec^{-1} (for T_e=1 eV), and the duration of the plasma current is $\sim 1/\nu_e \sim 200$ fsec. The dura-
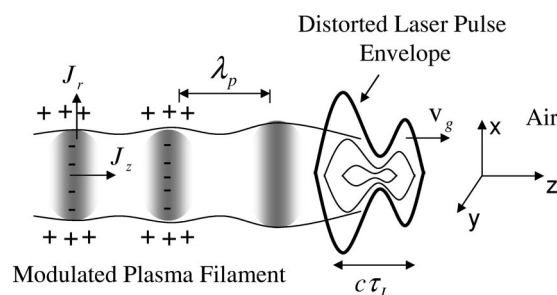

FIG. 1. Schematic diagram for atmospheric EMP generation. An ultrashort laser pulse ionizes the air and forms a plasma filament. The ponderomotive forces associated with the laser pulse envelope drive radial and axial currents, J_r and J_z, respectively, which are the source of EMP. The laser pulse distorts due to ionization and the optical Kerr effect. The filament is modulated at the plasma wavelength λ_p. The axial EMP electric field outside the filament is small due to shielding by surface charges at the air-plasma boundary.

*Present address: Icarus Research, Inc., P.O. Box 30780, Bethesda, MD 20824-0780, USA.

†Present address: LET Corp., 4431 MacArthur Blvd., Washington, DC 20007, USA.

tion of the EMP in air, at a fixed point, is a few hundred femtoseconds, i.e., the laser pulse duration plus the electron collision time. The spatial gradients associated with the laser pulse envelope as well as electron collisions lead to ponderomotive forces on the plasma electrons. These forces cause the electrons to oscillate, setting up plasma currents. The axial and transverse components of plasma current pulse have velocities close to the group velocity of the laser pulse. This is similar to the laser driven excitation of plasma waves in the laser wakefield accelerator (LWFA) [29]. In the LWFA plasma oscillations occur at the local plasma frequency. In general the various field components of the plasma oscillations are coupled, as are the axial and transverse plasma currents. These induced plasma currents, which travel with the laser pulse, are the source of the atmospheric EMP. The axial extent of the EMP is limited, and consequently, the spectrum of the EMP pulse can be broad. However, the characteristic frequency of the EMP measured outside of the plasma filament is determined by the laser pulse duration and not the local plasma frequency.

The results of our analysis for atmospheric EMP generation can be summarized as follows. For steady state propagation, in which the laser pulse and plasma filament are static in the group velocity frame of the laser pulse, the plasma current source travels with a velocity equal to the laser pulse group velocity. Since the group velocity is necessarily less than the speed of light, there is no EMP radiation generated. The absence of radial EMP emission in the steady state is one of several fundamental differences between our results and those of Cheng *et al.*, reported in Refs. [30,31].

In the model of Ref. [30], several assumptions were made which lead to incorrect conclusions. Of fundamental importance is the fact that in a steady state situation, it is not possible to generate a radiative field via an excitation which travels with a velocity less than the speed of light in the medium. Cheng *et al.* consider a steady state situation in which the driving laser pulse travels with a group velocity $v_g < c$. In this case, the driven response will have Fourier components with phase velocities equal to v_g, and therefore produces no radiation. Cheng *et al.*, inconsistently assume that the EMP source (plasma current) driven by the laser pulse is spatially uniform and oscillates in time at the plasma frequency. Effectively, they assume that the source has infinite phase velocity and, as a result, obtain a radiative field. In our model, the Fourier components of the plasma current in the steady state have phase velocities equal to the laser pulse group velocity, and therefore do not radiate. The absence of EMP in the steady state is analogous to the lack of Cherenkov radiation when the velocity of a charged particle is less than the velocity of light in the medium [32]. In addition to this, we consider the nonsteady state regime and derive conditions for radiation.

Cheng *et al.* retain the effect of radiation pressure from collisions but neglect the ponderomotive force on the electrons due to the gradient of the laser envelope. Their neglect of the ponderomotive force was based on an incorrect estimate of its magnitude. They incorrectly calculate the ponderomotive force based on the length of the plasma filament (~ 1 cm) instead of the length of the laser pulse (~ 3 μm). For their assumed parameters, the ponderomotive force is in fact much larger than the radiation pressure. In our model, we include the ponderomotive force, radiation pressure force, as well as a contribution due to ionization. The radial component of the plasma current in the filament can lead to surface charges on the plasma-air boundary. The surface charge density is strongly dependent on the collisionality of the plasma. In the weakly collisional regime the surface charge leads to greatly reduced EMP fields beyond the filament.

Under conditions of nonsteady state (transient) propagation, the plasma currents can generate EMP having a radial energy flux. For nonsteady state pulse propagation, the plasma currents can have Fourier components with phase velocities greater than the laser pulse group velocity. These Fourier components can generate radiative EMP, analogous to Cherenkov radiation. A condition for generating radiative EMP in the transient regime is derived and the differing characteristics of EMP in the steady state and transient propagation regimes are discussed in detail and illustrated with simulations. For typical atmospheric conditions and laser parameters it is found that the efficiency of the EMP generation from laser-atmospheric interaction, i.e., the ratio of the EMP energy to the laser pulse energy, is extremely small.

In addition to atmospheric EMP generation we consider EMP from the interaction of short laser pulses with dielectric surfaces. The source of the EMP on the surfaces of the dielectric is the oscillating plasma sheet formed by the ionization process as well as an optical rectification process. Our analysis of EMP generation on the surfaces of a dielectric indicates that the conversion efficiency is extremely small.

This paper is organized as follows. The general equations describing the evolution of the driving laser pulse and EMP in air are derived in Sec. II. Also in Sec. II, an estimate of the EMP power conversion efficiency is derived and an analysis of the steady state and transient propagation regimes presented. In Sec. III EMP generation from a dielectric surface on which a laser pulse is incident is analyzed. Section IV presents self-consistent numerical simulations showing laser pulse propagation, plasma filament formation, and EMP generation in air and on dielectric surfaces. A summary of the results and concluding remarks is found in Sec. V.

II. ELECTROMAGNETIC PULSE GENERATION IN AIR

In this section we derive the general equations for the generation of EMP radiation from laser-induced plasma currents in air. For the parameters of interest, the driving laser pulse intensity is sufficiently high that it partially ionizes the air and forms a plasma filament behind the laser pulse. An equation for the amplitude of the driving laser pulse is derived that includes the effects of diffraction, Kerr focusing, plasma defocusing, electron collisions, and laser pulse energy depletion caused by ionization. The plasma currents within the filament are driven by the ponderomotive forces associated with the laser pulse and are described by a set of cold fluid equations which include the effects of multiphoton ionization, electron-neutral elastic collisions, and electron recombination/attachment. In our model an axially symmetric laser-plasma configuration is assumed and stimulated Ra-

man scattering of the laser pulse and other instabilities are not considered [33,34].

A. Driving laser pulse

For a self-consistent description of EMP generation the spatial and temporal evolution of the driving laser pulse is needed. The ponderomotive forces, which are proportional to the energy density of the driving laser pulse, induce low frequency plasma currents which in turn generate EMP. The driving laser pulse is assumed to be many optical wavelengths long and to have a spot size that is large compared to the wavelength. The transverse laser fields are given by

$$\mathbf{E}_L(\mathbf{r},t) = E_L(\mathbf{r},t)\exp[i(k_0 z - \omega_o t)]\hat{\mathbf{e}}_x/2 + \text{c.c.}, \quad (1a)$$

$$\mathbf{B}_L(\mathbf{r},t) = B_L(\mathbf{r},t)\exp[i(k_0 z - \omega_o t)]\hat{\mathbf{e}}_y/2 + \text{c.c.}, \quad (1b)$$

where ω_o is the carrier frequency, $k_o = \omega_o/c$ is the wave number, $\hat{\mathbf{e}}_x(\hat{\mathbf{e}}_y)$ is a unit vector in the $x(y)$ direction, and c.c. denotes the complex conjugate. In Eq. (1a) E_L is the slowly varying complex electric field amplitude satisfying $|E_L^{-1}\partial E_L/\partial t| \ll \omega_o$ and $|E_L^{-1}\partial E_L/\partial z| \ll k_o$. The transverse magnetic field amplitude is $B_L \cong [1-i(c/\omega_0)(\partial/\partial z + c^{-1}\partial/\partial t)]E_L$. The axial electric and magnetic fields of magnitude $\sim(c/\omega_o)|\partial E_L/\partial x|$ and $\sim(c/\omega_o)|\partial E_L/\partial y|$, respectively, which are associated with the transverse laser fields in Eqs. (1), are small and are neglected.

Making use of the electron cold fluid equations, the transverse current density $\mathbf{J}_L = q\, n_e \mathbf{v}_L$ induced by the laser pulse is given by

$$\frac{\partial \mathbf{J}_L}{\partial t} + \nu_e \mathbf{J}_L = \frac{\omega_p^2(\mathbf{r},t)}{4\pi}\mathbf{E}_L, \quad (2)$$

where $\nu_e = \nu_{en} + \nu_{ei}$ is the electron collision frequency, ν_{en} is the electron-neutral collision frequency, ν_{ei} is the electron-ion collision frequency, $\omega_p(\mathbf{r},t) = [4\pi q^2 n_e(\mathbf{r},t)/m]^{1/2}$ is the local plasma frequency, q is the electronic charge, $\mathbf{v}_L$ is the quiver velocity in the laser field, and n_e is the electron density in the plasma filament which is formed by photoionization. It is assumed that the ions are immobile on the time scale of interest. In general, the electron density n_e includes contributions from plasma oscillations as well as the ionization process. The solution of Eq. (2) for the first-order transverse current density induced by the laser field is

$$\mathbf{J}_L(\mathbf{r},t) = J_L(\mathbf{r},t)\exp[i(k_o z - \omega_o t)]\hat{\mathbf{e}}_x/2 + \text{c.c.}, \quad (3)$$

where $J_L \cong (i/4\pi\omega_o)[1-(i/\omega_o)(\partial/\partial t + \nu_e)](\omega_p^2 E_L)$, where we have assumed that $\omega_o \gg \nu_e$.

The electron-neutral collision frequency is given by $\nu_{en} = n_n\sigma_0(k_B T_e/m)^{1/2}$, where $n_n = n_{no} - n_e$ is the neutral density (singly ionized plasma), n_{no} is the ambient neutral density, k_B is the Boltzmann constant, and $\sigma_0 \approx 5 \times 10^{-15}$ cm^2 is a typical value for the scattering cross section [35]. In practical units the expression can be written as $\nu_{en}[\text{sec}^{-1}] \approx 2 \times 10^{-7} n_n\,[\text{cm}^{-3}](T_e[\text{eV}])^{1/2}$. For a neutral air density of $n_n = n_{no} = 2.7 \times 10^{19}$ cm^{-3} and temperature $T_e = 1$ eV, the electron collision frequency is $\nu_{en} \approx 5.7 \times 10^{12}$ sec^{-1}. Note that for a plasma density of $n_e \sim 10^{16}$ cm^{-3}, the electron-neutral

collision frequency and plasma frequency are comparable, $\nu_{en} \sim \omega_p$. Taking the Coulomb logarithm to be equal to 10, the electron-ion collision frequency [35] is $\nu_{ei}[\text{sec}^{-1}] \approx 3 \times 10^{-5} n_i[\text{cm}^{-3}](T_e[\text{eV}])^{-3/2}$, for singly ionized plasma, i.e., $n_e = n_i$. In an intense laser field the electron temperature in the expressions for ν_{en} and ν_{ei} must be replaced by the laser oscillation energy.

1. Plasma current

The propagation of the driving laser pulse is strongly influence by the plasma filament. The plasma dynamics are described by the nonrelativistic, cold fluid equations

$$\frac{\partial n_e}{\partial t} + \boldsymbol{\nabla} \cdot (n_e\mathbf{v}) = \nu_{ion}n_n - \beta_{recom}\, n_e^2 - \beta_{attach}n_e n_n^2, \quad (4a)$$

$$\begin{aligned}\frac{\partial \mathbf{v}}{\partial t} + (\mathbf{v}\cdot\boldsymbol{\nabla})\mathbf{v} &= \frac{q}{m}\left(\mathbf{E} + \frac{\mathbf{v}\times\mathbf{B}}{c}\right) - \nu_e\mathbf{v} \\ &\quad - \left(\frac{\partial n_e}{\partial t} + \boldsymbol{\nabla}\cdot(n_e\mathbf{v})\right)\mathbf{v}/n_e,\end{aligned} \quad (4b)$$

where $\mathbf{v}$ is the electron fluid velocity, ν_{ion} is the ionization rate, β_{recom} is the recombination coefficient, and β_{attach} is the attachment coefficient. In obtaining Eq. (4) we have assumed that the electrons immediately after ionization have zero velocity, i.e., the electrons are born at rest and above threshold ionization effects are ignored.

For the parameters of interest here the ionization process is principally due to multiphoton ionization and the corresponding rate can be fitted analytically by [36]

$$\nu_{ion} = \frac{2\pi\omega_o}{(\ell-1)!}\left(\frac{I_L(r,z,t)}{I_{MP}}\right)^\ell, \quad (5)$$

where the integer $\ell \leq \text{int}(U_{ion}/\hbar\omega_o + 1)$ refers to the effective number of photons absorbed by the molecule in the ionization process, U_{ion} is the ionization energy, I_L is the laser intensity, and $I_{MP} = \hbar\omega_o^2/\sigma_{MP}$, with σ_{MP} an empirically determined ionization cross section. At laser intensities of $\sim 10^{14}$ W/cm^2 or above tunneling ionization becomes important. For a laser wavelength of $\lambda_o = 0.8\ \mu$m($\hbar\,\omega_o = 1.54$ eV) in air, the multiphoton ionization order of O$_2$ is $\ell = 8$, and the characteristic intensity is determined empirically to be $I_{MP} \sim 10^{14}$ W/cm^2 for pulses with durations ~ 100 fsec [16]. Since the intensity ratio in Eq. (5) is raised to the eighth power, the ionization rate is an exceedingly sensitive function of the laser intensity and the value of the parameter I_{MP}. The scaling of the ionization rate in Eq. (5) with laser intensity is the same as that given in Ref. [37]. Since the numerical value of the Keldysh formula in Ref. [37] differs from the experimental value, we use the empirical cross section quoted above. A similar approach was adopted in Ref. [38] to obtain an empirical formula for the multiphoton ionization rate. For a laser intensity of $I_L = 7 \times 10^{13}$ W/cm^2, laser wavelength of $\lambda_o = 0.8\ \mu$m($\omega_o = 2.4 \times 10^{15}$ sec^{-1}), and ionization order of $\ell = 8$, the ionization rate is $\nu_{ion} \sim 2 \times 10^{11}$ sec^{-1}. The ionization rate, however, is an extremely sensitive function of the laser intensity. The recombination time is given by

$\tau_{recom} = 1/\beta_{recom} n_e$. Taking $\beta_{recom}[\mathrm{cm^3/sec}] \approx 2 \times 10^{-8}(T_e[\mathrm{eV}])^{-1/2}$ [14], $n_e = 10^{16}$ cm^{-3}, and $T_e = 1$ eV, the recombination time $\tau_{recom} \sim 5$ nsec. The attachment coefficient β_{attach} of electrons on oxygen molecules is discussed in Ref. [39]. For an electron temperature of ~ 1 eV the attachment coefficient is $\beta_{attach} \sim 3.4 \times 10^{-31}$ cm^6/sec and the attachment time is $\tau_{attach} = 1/\beta_{attach} n_n^2 \sim 4$ nsec. The duration of the plasma filament is on the order of the shorter of the two time scales, τ_{recom} and τ_{attach}, i.e., $\min[\tau_{recom}, \tau_{attach}]$.

Combining Eqs. (4a) and (4b) results in an equation for the electron plasma current density, $\mathbf{J} = q\, n_e \mathbf{v}$, given by [40]

$$\frac{\partial \mathbf{J}}{\partial t} + \nu_e \mathbf{J} = \frac{\omega_p^2}{4\pi} \mathbf{E} + \mathbf{S},\tag{6}$$

where $\mathbf{S}(r,z,t)$ is the nonlinear driving term. The first term on the right-hand side of Eq. (6) is associated with collective effects while the second term represents the driving ponderomotive force due to the laser pulse. The duration of the plasma current density is limited to $\sim 1/\nu_e \sim 200$ fsec for $n_e = 10^{16}$ cm^{-3}. To second order in the laser field amplitude,

$$\mathbf{S} = \frac{q}{mc} \mathbf{J}_L \times \mathbf{B}_L - q^{-1}(\boldsymbol{\nabla} \cdot \mathbf{J}_L)\mathbf{J}_L/n_e - q^{-1}(\mathbf{J}_L \cdot \boldsymbol{\nabla})(\mathbf{J}_L/n_e).\tag{7}$$

When the laser spot size is large compared to the plasma filament spot size, i.e., $R_o \gg r_p$, the ponderomotive source term in Eq. (7) can be simplified. This is a valid approximation in the case of higher order multiphoton ionization where the ionization rate is a strong function of laser intensity. In this limit the axial component of the source term S_z is given by

$$S_z(r,z,t) \approx -\frac{q}{16\pi m}\frac{\omega_p^2(r,z,t)}{\omega_o^2}\left(\frac{\partial}{\partial z} - \frac{2\nu_e}{c} - \frac{2}{c\omega_p^2}\frac{\partial \omega_p^2}{\partial t}\right) \times |E_L(r,z,t)|^2.\tag{8}$$

Note that the axial source term contains the ponderomotive force due to the spatial gradient of the laser pulse envelope, radiation pressure due to electron collisions, as well as changes in the electron density from ionization. The transverse component of the source term, for the laser pulse linearly polarized in the x direction, is

$$\mathbf{S}_\perp \approx -\frac{q}{16\pi m}\frac{\omega_p^2(r,z,t)}{\omega_o^2}\left(\hat{\mathbf{e}}_r\frac{\partial}{\partial r} + \hat{\mathbf{e}}_x\frac{2}{\omega_p^2}\frac{\partial \omega_p^2}{\partial x}\right)|E_L(r,z,t)|^2,\tag{9}$$

where $\hat{\mathbf{e}}_r$ is a unit vector in the radial direction. Note that the transverse part of the source term has a component in the x direction. For a circularly polarized laser pulse the axial component of the source term is given by Eq. (8) with E_L replaced with $\sqrt{2}E_L$ and the transverse component is purely radial and given by

$$\mathbf{S}_\perp \approx -\frac{q}{8\pi m}\frac{\omega_p^2(r,z,t)}{\omega_o^2}\left(\frac{\partial}{\partial r} + \frac{1}{\omega_p^2}\frac{\partial \omega_p^2}{\partial r}\right)|E_L(r,z,t)|^2 \hat{\mathbf{e}}_r.\tag{10}$$

The axially symmetric circularly polarized laser field has been assumed to be of the form $\mathbf{E}_L = E_L \exp[i(k_o z - \omega_o t)](\hat{\mathbf{e}}_x - i\hat{\mathbf{e}}_y)/2 + \text{c.c.}$

2. Laser pulse amplitude

To obtain the ponderomotive source term self-consistently, an equation describing the evolution of the driving laser pulse is needed. For this purpose it is useful to transform to the group velocity frame in which the independent variables are z and $\tau = t - z/v_g$, where v_g denotes the linear group velocity of the laser pulse, and is defined later. In terms of the new independent variables (z,τ) the derivatives are given by $\partial/\partial t \rightarrow \partial/\partial \tau$ and $\partial/\partial z \rightarrow \partial/\partial z - v_g^{-1}\partial/\partial \tau$. In the variables (z,r,τ) the laser pulse evolves slowly, i.e., is nearly stationary. The wave equation for the complex laser amplitude $E_L(r,z,\tau)$ in the new independent variables takes the form [36]

$$\frac{\partial E_L(r,z,\tau)}{\partial z} = \frac{i}{2}\frac{c}{\omega_o}\left[\nabla_\perp^2 + \frac{\omega_o^2 n_K}{4\pi c}\frac{n_n}{n_{no}}|E_L|^2 - \frac{\omega_{po}^2(r,z,\tau)}{c^2}\right.$$
$$\left.\times\left(1 - i\frac{\nu_e}{\omega_o}\right) + 8\pi i\frac{\omega_o}{c^2}\frac{U_{ion}}{|E_L|^2}\frac{\partial n_{eo}}{\partial \tau}\right]E_L(r,z,\tau).\tag{11}$$

The first term on the right-hand side of Eq. (11) is the Laplacian operator which is responsible for diffractive spreading of the laser beam. The second term is proportional to the nonlinear Kerr refractive index n_K and can lead to nonlinear self-focusing [40,41]. The terms proportional to ω_{po}^2 represent the effect of plasma defocusing and collisions [36,40]. The last term describes laser pulse energy depletion due to ionization of the air molecules with effective ionization energy U_{ion}. In general the refractive index for electromagnetic waves in a medium consists of contributions from the linear and the nonlinear polarization field. In the present analysis it is assumed that the contribution to the nonlinear refractive index is proportional to the laser intensity, i.e., Kerr effect. This is a valid approximation for a gas as well as for an amorphous dielectric. For the laser pulse this nonlinear contribution to the index leads to the phenomena of nonlinear Kerr self-focusing.

3. Source dependent expansion analysis of laser pulse

Equation (11) for the laser pulse amplitude can be approximately solved by employing the source dependent expansion (SDE) method [42]. In this method the laser field is assumed to have a Gaussian transverse profile

$$|E_L(r,z,\tau)| = |E_L(0,z,\tau)|\exp[-r^2/R^2(z,\tau)],\tag{12}$$

where R is the laser spot size. For the Gaussian transverse profile the laser power is

$$P_L(z,\tau) = c|E_L(0,z,\tau)|^2 R^2(z,\tau)/16. \tag{13}$$

Employing the SDE method results in coupled equations for the spot size and power,

$$\frac{\partial^2 R(z,\tau)}{\partial z^2} - \frac{4c^2}{\omega_o^2}\frac{1}{R^3(z,\tau)}\left(1 - \frac{P_L(z,\tau)}{P_K}\right.$$
$$\left. + \frac{2\pi\ell r_e\, n_{eo}(0,z,\tau)}{(\ell+1)^2}R^2(z,\tau)\right) = W(z,\tau), \tag{14a}$$

$$\frac{\partial P_L(z,\tau)}{\partial z} = -\frac{1}{\ell+1}\frac{\omega_{po}^2(0,z,\tau)}{\omega_o^2}\frac{\nu_e}{c}P_L(z,\tau)$$
$$- \frac{\pi}{2\ell}U_{ion}\nu_{ion}n_n R^2(z,\tau), \tag{14b}$$

where $P_K = \lambda_o^2/(2\pi\, n_K\, n_n/n_{no})$ is the nonlinear Kerr focusing power, $r_e = q^2/mc^2$ is the classical electron radius, and

$$W(z,\tau) = -\frac{1}{R}\left(\frac{\partial}{\partial z}(R^2 U) + R^2 U^2\right), \tag{15a}$$

$$U(z,\tau) = \frac{(\ell-1)}{2\ell}\frac{1}{P_L}\frac{\partial P_L}{\partial z} - \frac{1}{2\ell(\ell+1)^2}\frac{\omega_{po}^2}{\omega_o^2}\frac{\nu_e}{c}, \tag{15b}$$

$$\frac{\partial n_{eo}}{\partial \tau} = \nu_{ion}n_n. \tag{15c}$$

The decrease in the total laser pulse power as a function of propagation distance is due to both collisional absorption and ionization. The evolution of the total laser pulse power given by Eq. (14b) can be rewritten as

$$\frac{\partial P_L(z,\tau)}{\partial z} = -\left(\frac{1}{L_{coll}} + \frac{1}{L_{ion}}\right)P_L(z,\tau), \tag{16}$$

where

$$L_{coll} = (\ell+1)\frac{\omega_o^2}{\omega_{po}^2}\frac{c}{\nu_e} \tag{17a}$$

is the absorption length due to collisional effects and

$$L_{ion} = \frac{2\ell}{\pi}\frac{P_L}{U_{ion}\nu_{ion}n_n R^2} \tag{17b}$$

is the absorption length due to ionization effects. It should be noted that due to the nonlinear character of Eq. (16), the expressions in Eqs. (17a) and (17b) are at best local estimates for the scale lengths. As an example, consider the case of a laser pulse having a power $P_L = 0.1$ TW, wavelength $\lambda_o = 0.8$ μm, pulse duration $\tau_L = 100$ fsec, intensity $I_L = 5 \times 10^{13}$ W/cm^2, and spot size $R \sim 360$ μm, propagating in air with a neutral density $n_{no} = 2.7 \times 10^{19}$ cm^{-3}, effective ionization energy of $U_{ion} = 8$ eV($\ell=8$), and electron collision frequency of $\nu_e = \nu_{en} + \nu_{ei} \approx 6 \times 10^{12}$ sec^{-1}. In this case the ionization rate is $\nu_{ion} \sim 10^{10}$ sec^{-1}($I_{MP} = 10^{14}$ W/cm^2) and the electron density is $n_e \sim 3 \times 10^{16}$ cm^{-3}, ($\omega_o/\omega_{po} \sim 230$). For these parameters the collisional absorption length is L_{coll}

~ 25 m while the ionization absorption length is $L_{ion} \sim 10$ m. In this example, the laser pulse propagation distance is limited by ionization absorption. It should be stressed that these characteristic scale lengths are very sensitive functions of the laser and plasma parameters.

4. Pulse group velocity

The group velocity is given by $v_g = c(n + \omega_o\, \partial n/\partial\omega_o)^{-1}$, where n is the total refractive index and expressible as

$$n \cong n_o - \frac{f\omega_{po}^2}{2\omega_o^2} - \frac{2c^2}{\omega_o^2 R_o^2} + n_K I_L. \tag{18}$$

Here R_o is the initial spot size of the laser pulse, and $I_L = cn_o|E_L|^2/8\pi$ is the time-averaged laser intensity. The filling factor f is the ratio of the plasma filament cross sectional area to the laser pulse cross sectional area. Using the expression for the plasma density due to the multiphoton ionization process in Eq. (5) we find that $f \sim (\ell+1)^{-1}$. The filling factor is necessary for calculating the correct group velocity of the laser pulse in the presence of the plasma filament. The third term on the right-hand side of Eq. (18) denotes the correction to the refractive index due to the finite spot size of the laser pulse and the fourth term represents the nonlinear index due to the Kerr effect. Making use of the expression for the refractive index, the group velocity $v_g = c\beta_g = 1/[n + \partial(\omega_o n)/\partial\omega_o]$ is expressible as

$$\beta_g \cong \frac{1}{n_o} - \frac{f\omega_{po}^2}{2\omega_o^2} - \frac{2c^2}{\omega_o^2 R_o^2} - n_K I_L. \tag{19}$$

In deriving Eq. (19), it is assumed that the variation of the linear index and Kerr index with frequency is negligible. For $I_L = 10^{14}$ W/cm^2, $R_o = 260$ μm, $\lambda_o = 0.8$ μm, $n_e = 10^{16}$ cm^{-3}, $n_K = 6 \times 10^{-19}$ cm^2/W, and $\ell = 8$, the magnitudes of the plasma, finite spot size, and optical Kerr contributions to β_g are $\sim 3 \times 10^{-7}$, 3×10^{-6}, and $\sim 6 \times 10^{-5}$, respectively.

B. EMP equations in air

The wave equation for the EMP electric field **E** in air which is driven by plasma currents is given by

$$\mathbf{\nabla} \times (\mathbf{\nabla} \times \mathbf{E}) + \frac{n_o^2}{c^2}\frac{\partial^2 \mathbf{E}}{\partial t^2} = -\frac{4\pi}{c^2}\frac{\partial \mathbf{J}}{\partial t}, \tag{20}$$

where n_0 is the linear refractive index and the plasma current is given by Eq. (6). We use a cylindrical coordinate system where r, θ, and z denote the radial coordinate, azimuthal angle, and axial coordinate, respectively, and assume axial symmetry, i.e., $\partial/\partial\theta = 0$. The generation of EMP from the surface of dielectrics is analyzed in Sec. III. In the laser pulse group velocity frame, the axial and radial components of the EMP electric field are given by

$$\left[\frac{1}{r}\frac{\partial}{\partial r}\left(r\frac{\partial}{\partial r}\right) - \frac{1}{c^2}\frac{\partial^2}{\partial \tau^2}\right]E_z + \left(\frac{1}{v_g}\frac{\partial}{\partial \tau} - \frac{\partial}{\partial z}\right)\frac{1}{r}\frac{\partial}{\partial r}(r\, E_r)$$
$$= \frac{4\pi}{c^2}\frac{\partial J_z}{\partial \tau}, \tag{21a}$$

$$\left(\frac{1}{v_g^2 \, \gamma_g^2} \frac{\partial^2}{\partial \tau^2} - \frac{2}{v_g} \frac{\partial^2}{\partial z \, \partial \tau} + \frac{\partial^2}{\partial z^2} \right) E_r + \left(\frac{1}{v_g} \frac{\partial}{\partial \tau} - \frac{\partial}{\partial z} \right) \frac{\partial E_z}{\partial r}$$

$$= \frac{4\pi}{c^2} \frac{\partial J_r}{\partial \tau}, \tag{21b}$$

where $\gamma_g \equiv (1 - n_0^2 v_g^2 / c^2)^{-1/2}$. Using Eq. (19) γ_g is found to be given by

$$\gamma_g \cong \omega_o / (f \, \omega_{po}^2 + 4c^2/R_o^2 + 2\omega_o^2 \, n_K \, I_L)^{1/2}. \tag{22}$$

For $\lambda_o = 0.8$ μm, $n_e = 10^{17}$ cm^{-3}, $n_K = 6 \times 10^{-19}$ cm^2/W, $I_L = 10^{14}$ W/cm^2, $\ell = 8$, and $R_o = 260$ μm, we find that the plasma wavelength $\lambda_p = 2\pi c/\omega_p \sim 106$ μm and $\gamma_g \approx 90$.

Taking the Fourier transform of Eqs. (21a) and (21b) together with Eq. (6) in the variables z and τ, with the convention $Q = (2\pi)^{-1} \int_{-\infty}^{\infty} \tilde{Q} \exp(ikz - i\omega\tau) dk \, d\omega$, gives

$$\left[\frac{1}{r} \frac{\partial}{\partial r} \left(r \frac{\partial}{\partial r} \right) + \frac{\omega^2}{c^2} - \frac{\omega_p^2(r)}{c^2(1 + i\nu_e/\omega)} \right] \tilde{E}_z$$

$$- i \left(\frac{\omega}{v_g} + k \right) \frac{1}{r} \frac{\partial}{\partial r} (r \, \tilde{E}_r) = \frac{4\pi}{c^2} \frac{\tilde{S}_z(r,k,\omega)}{1 + i\nu_e/\omega}, \tag{23a}$$

$$\left(k^2 + \frac{2k\omega}{v_g} + \frac{\omega^2}{v_g^2 \gamma_g^2} + \frac{\omega_p^2(r)}{c^2(1 + i\nu_e/\omega)} \right) \tilde{E}_r + i \left(\frac{\omega}{v_g} + k \right) \frac{\partial \tilde{E}_z}{\partial r}$$

$$= -\frac{4\pi}{c^2} \frac{\tilde{S}_r(r,k,\omega)}{1 + i\nu_e/\omega}. \tag{23b}$$

The azimuthal magnetic field is given by

$$\tilde{B}_\theta = \left(1 - \frac{\omega_p^2(r)}{\omega^2(1 + i\nu_e/\omega)} \right) \left(1 + \frac{k \, v_g}{\omega} \right)^{-1} \tilde{E}_r$$

$$- \frac{4\pi}{c^2} \left(1 + \frac{k \, v_g}{\omega} \right)^{-1} \frac{\tilde{S}_r(r,k,\omega)}{1 + i\nu_e/\omega}. \tag{24}$$

In obtaining Eqs. (23) we have set n_o equal to unity. In the following section Eqs. (23) and (24) are solved analytically for an idealized plasma filament.

C. Analysis of EMP in air

We consider steady state and nonsteady state (transient) propagation of the laser pulse for an idealized case that can be solved analytically. The laser pulse envelope is taken to have the form

$$|E_L(0,z,\tau)| = \hat{E}_L(z) \sin(\pi \, \tau/\tau_L) \tag{25}$$

for $0 \le \tau \le \tau_L$ and $E_L = 0$ otherwise. The front of the laser pulse is at $\tau = 0$ and the back is at $\tau = \tau_L$. We analyze Eqs. (23) and (24) for the case of an idealized plasma filament with radial extent r_p in which the plasma density is constant for $r < r_p$ and zero for $r > r_p$. It is also assumed that the recombination process is negligible and that the ionization process is sufficiently rapid that the plasma density does not vary longitudinally within and behind the laser pulse, i.e., ω_p is independent of τ. Under these assumptions, Eqs. (23a) and (23b) can be combined to give equations for the axial field

inside ($r < r_p$) and outside ($r > r_p$) the plasma filament, respectively,

$$\left[\frac{1}{r} \frac{\partial}{\partial r} \left(r \frac{\partial}{\partial r} \right) - \kappa_p^2(\omega,k) \right] \tilde{E}_z$$

$$= -\frac{4\pi}{\omega^2(1 + i\nu_e/\omega) - \omega_{po}^2} \left(\kappa_p^2(\omega,k) \tilde{S}_z(r,\omega,k) \right.$$

$$\left. - (\omega/v_g + k) \frac{1}{r} \frac{\partial}{\partial r} [r \tilde{S}_r(r,k,\omega)] \right), \tag{26a}$$

$$\left[\frac{1}{r} \frac{\partial}{\partial r} \left(r \frac{\partial}{\partial r} \right) - \kappa_o^2(\omega,k) \right] \tilde{E}_z = 0, \tag{26b}$$

where

$$\kappa_o^2(\omega,k) = \frac{\omega^2}{v_g^2 \gamma_g^2} + \frac{2\omega k}{v_g} + k^2, \tag{27a}$$

$$\kappa_p^2(\omega,k) = \kappa_o^2(\omega,k) + \frac{\omega_{po}^2}{c^2(1 + i\nu_e/\omega)}, \tag{27b}$$

and ω_{po} denotes the constant plasma frequency within the channel. The radial component of the source term, i.e., $\tilde{S}_r$, can be neglected provided $\omega_{po} r_p/c \gg 1$. This is assumed to be the case in writing Eqs. (26) and (27). However, in the numerical simulations the radial source term is not necessarily neglected.

The boundary conditions across the plasma-air interface at $r = r_p$ are the continuity of the axial electric field, $\tilde{E}_z(r = r_p^-) = \tilde{E}_z(r = r_p^+)$, and the azimuthal magnetic field $\tilde{B}_\theta(r = r_p^-) = \tilde{B}_\theta(r = r_p^+)$. Applying the boundary conditions, the axial electric fields inside and outside the plasma filament are, respectively,

$$\tilde{E}_z(r,\omega,k) = \frac{4\pi \tilde{S}_z(\omega,k)}{\omega^2(1 + i\nu_e/\omega) - \omega_{po}^2} \left(1 - \frac{\kappa_o \, r_p \, K_1(\kappa_o r_p)}{D(\omega,k)} I_o(\kappa_p r) \right), \tag{28a}$$

$$\tilde{E}_z(r,\omega,k) = \frac{4\pi \tilde{S}_z(\omega,k)}{\omega^2(1 + i\nu_e/\omega)} \frac{\kappa_o \, r_p \, I_1(\kappa_p r_p)}{D(\omega,k)} \left(\frac{\kappa_0}{\kappa_p} \right) K_o(\kappa_o r), \tag{28b}$$

where I_o and K_o are the modified Bessel functions of order zero of the first and the second kind, respectively,

$$D(\omega,k) = h(\omega,k) \kappa_p r_p K_o(\kappa_o r_p) I_1(\kappa_p r_p)$$

$$+ \kappa_o r_p \, K_1(\kappa_o r_p) I_o(\kappa_p r_p) \tag{29a}$$

and

$$h(\omega,k) = \left(1 - \frac{\omega_{po}^2}{\omega^2(1 + i\nu_e/\omega)} \right) \frac{\kappa_o^2(\omega,k)}{\kappa_p^2(\omega,k)}. \tag{29b}$$

Making use of Eqs. (28a) and (28b) the ratio of the field at the boundary to the field at the center of the filament is

$$\frac{\widetilde{E}_z(r=r_p)}{\widetilde{E}_z(r=0)} = \frac{h(\omega,k)\kappa_p r_p\, I_1(\kappa_p r_p) K_o(\kappa_o r_p)}{D(\omega,k) - \kappa_o r_p K_1(\kappa_o r_p)}. \tag{30}$$

In the plasma filament there is a radial component of plasma current density that induces a surface charge at the plasma-air boundary. The resulting charge distribution is such that the EMP fields outside the filament are extremely small. Neglecting the radial source term $\mathbf{S}_r$ in Eq. (24), continuity of the azimuthal magnetic field across the boundary implies that

$$\frac{\widetilde{E}_r(r=r_p^+)}{\widetilde{E}_r(r=r_p^-)} = 1 - \frac{\omega_{po}^2}{\omega^2(1+i\,\nu_e/\omega)}. \tag{31}$$

In the weakly collisional regime ($\nu_e \ll \omega$) and for $\omega \sim \omega_p$ it follows that the field outside is nearly completely shielded. In the highly collisional regime, however, the EMP field is not shielded outside the filament.

In Sec. II C 2 and II C 3 we analyze and discuss limiting cases of these equations for comparison with the numerical results.

1. Estimate of EMP power conversion efficiency

A rough estimate for the efficiency of converting laser power to EMP power can be obtained by using rather general arguments concerning the EMP field amplitudes. This provides a consistency check with the calculation of efficiency obtained by the far more precise analysis which follows. In addition, this estimate shows that the low efficiencies obtained by more precise analysis are to be expected.

The maximum amplitude of the longitudinal electric field (wakefield) induced by the driving laser pulse propagating in the plasma filament in the absence of collisions is given by [29]

$$E_{z,\max} \approx \frac{\pi^2}{2}\frac{mc^2}{q}\frac{a_L^2}{c\tau_L}, \tag{32}$$

where $a_L = q|E_L|/m\,c\,\omega_o$ is the laser strength parameter. The frequency of the wakefield is in the THz range and determined by the laser pulse duration τ_L. In the absence of collisions, the maximum field amplitude occurs when the laser pulse duration is approximately equal to the plasma frequency $\omega_p\,\tau_L \sim 1$ [29]. The other components of the EMP fields induced by the driving laser pulse are of the same order or smaller than the above maximum axial field. The power in the EMP is estimated to be $P_{EMP} \sim c\,E_{z,\max}^2\,\Sigma/8\pi$, where Σ is the area through which the EMP energy flows. The area of the cylinder enclosing the EMP fields is estimated to be $\Sigma \approx \pi(2\,N_p\,r_p\,c\,\tau_L + r_p^2)$, where N_p is the number of periods (i.e., plasma wavelengths) of the wakefield behind the laser pulse. The parameter N_p is a measure of the axial extent of the emitting region of the EMP. Typically, the plasma frequency is on the order of the electron collision frequency and consequently, $N_p \sim 1$. The driving laser pulse power can be written in terms of the laser strength parameter, $P_L = (c/16)(m\,c\,\omega_o R/q)^2 a_l^2$. Using Eq. (32) and the expression for the laser power we find that an estimate for the EMP power efficiency is

$$\eta_{power} = \frac{P_{EMP}}{P_L} \sim \frac{\pi^2}{8}\left(\frac{a_L\,\lambda_o}{c\,\tau_L}\right)^2\left(\frac{2\,N_p\,r_p\,c\,\tau_L + r_p^2}{R^2}\right), \tag{33}$$

where λ_o is the laser wavelength. As an illustration, consider a laser pulse intensity of $I_L = 7\times10^{13}$ W/cm^2 and wavelength $\lambda_o = 0.8$ μm, the laser strength parameter for these values is $a_L = 5.7\times10^{-3}$. For a laser pulse duration of $\tau_L = 250$ fsec, the power efficiency is

$$\eta_{power} \sim 2\times10^{-8}\left(\frac{2\,N_p\,r_p\,c\,\tau_L + r_p^2}{R^2}\right). \tag{34}$$

Taking the laser spot to be $R = 200$ μm, plasma filament spot size to be $r_p = 100$ μm, number of plasma wavelengths behind the pulse to be $N_p \sim 1$, the efficiency is extremely small, $\eta_{power} \sim 10^{-8}$. This estimate is typical of the values obtained by numerically solving the full set of EMP equations.

2. EMP in the steady state regime

In the steady state propagation regime it is assumed that both the plasma density and the laser pulse are independent of the propagation distance, i.e., $\partial\omega_{po}^2/\partial z = \partial|\hat{E}_L|^2/\partial z = 0$. Even in a homogeneous medium there is a minimum propagation distance needed to reach a steady state. The steady state EMP propagates with velocity equal to the group velocity of the laser pulse, v_g. The transient EMP on the other hand propagates with velocity $\sim c/n_o$. The propagation distance needed to reach a steady state is $L_{steady\ state} \sim \tau_L/|1/v_g - n_o/c| \sim 2\,\gamma_g^2\,c\,\tau_L$. For the purpose of illustration it will be assumed that the collision frequency can be neglected.

The axial EMP electric field is vanishingly small outside of the plasma filament, while inside the filament it is given by

$$\widetilde{E}_z(r,\omega) = \frac{4\,\pi\,\widetilde{S}_z(\omega)}{\omega^2 - \omega_{po}^2}\left(1 - \frac{I_o(\kappa_p r)}{I_o(\kappa_p\,r_p)}\right). \tag{35}$$

The EMP magnetic field inside and outside of the plasma filament is given by

$$\widetilde{B}_\theta(r,\omega) = \frac{4\,\pi\,i\,\widetilde{S}_z(\omega)}{\omega}\frac{I_1(\kappa_p\,r)}{c\,\kappa_p\,I_o(\kappa_p\,r_p)} \tag{36a}$$

and

$$\widetilde{B}_\theta(r,\omega) = \frac{4\,\pi\,i\,\widetilde{S}_z(\omega)}{\omega}\frac{I_1(\kappa_p\,r_p)}{c\,\kappa_p\,I_o(\kappa_p\,r_p)}\frac{K_1(\kappa_o\,r)}{K_1(\kappa_o\,r_p)}, \tag{36b}$$

respectively. For typical parameters we find that $\kappa_p r_p \sim \omega_{po}r_p/c \gg 1$ and $\kappa_o r_p \sim \omega\,r_p/(c\,\gamma_g) \ll 1$ and the EMP magnetic field inside and outside the plasma filament reduces to

$$\widetilde{B}_\theta(r,\omega) = \frac{4\,\pi\,i\,\widetilde{S}_z(\omega)}{\omega}\frac{1}{c}\left(\frac{2\,\pi\,c\,r_p}{\omega_{po}}\right)^{1/2}$$
$$\times\exp(-\omega_{po}r_p/c)I_1(\omega_{po}\,r/c), \tag{37a}$$

$$\widetilde{B}_\theta(r,\omega) = \frac{4\pi i\, \widetilde{S}_z(\omega)}{\omega_{po}} \frac{r_p}{v_g\, \gamma_g} K_1(\omega\, r/v_g\, \gamma_g). \quad (37b)$$

In the steady state and in the absence of collisions the Fourier transform of the source term in Eq. (8) is

$$\widetilde{S}_z(\omega) = -\frac{i\,q}{2\,m\,c} \frac{\omega}{c} \frac{\omega_{po}^2}{\omega_o^2} \widetilde{I}_L(\omega), \quad (38)$$

where $I_L(\tau) = c|E_L|^2/8\pi$ is the laser intensity.

To obtain the temporal variation of the fields it is necessary to invert the corresponding Fourier transforms. To derive an analytic expression for $B_\theta(r,\tau)$ we assume an intensity profile $I_L(\tau) = I_{L0}$ for $0 < \tau < \tau_L$ and zero otherwise. Substituting Eq. (38) into Eq. (36a) and (36b) and taking the inverse Fourier transform results in

$$B_\theta(r,\tau) = B_o \frac{r_p}{r} H(r,\tau), \quad (39)$$

where

$$H(r,\tau) = \frac{1}{2} \left(\frac{\tau}{[(r/v_g\gamma_g)^2 + \tau^2]^{1/2}} - \frac{(\tau - \tau_L)}{[(r/v_g\gamma_g)^2 + (\tau - \tau_L)^2]^{1/2}} \right), \quad (40a)$$

and

$$B_o = \frac{2\pi q}{m\,c^2} \frac{\omega_{po}}{\omega_o^2} I_{L0} \quad (40b)$$

is the peak magnetic field at $r=r_p$ and $\tau=\tau_L$. Note that the magnetic field in Eq. (39) is proportional to the square root of the plasma density. This dependence is due to the near cancellation of the axial components of the convective and inductive current densities. Evaluating the magnetic field at $r=r_p$ in Eq. (37a) and noting that $\omega_{po}\, r_p/c \gg 1$, we obtain $\widetilde{B}_\theta(r_p) = 4\pi i\, \widetilde{S}_z(\omega)/(\omega_{po}\omega)$. The inverse transform of this expression leads to the magnetic field given in Eq. (40b).

As an example consider the laser and plasma parameters $r_p\omega_{po}/c = 25$, $\tau_L\omega_{po}/2\pi = 0.8$, $\omega_o/\omega_{po} = 125$, $\ell = 8$, $\gamma_g \approx 140$, $\lambda_o = 0.8\ \mu$m ($\lambda_p = 100\ \mu$m), and peak laser intensity $I_{L0} = 7 \times 10^{13}$ W/cm². For these parameters the magnetic field at the surface of the filament is $B_o \approx 9$ G. The axial flux is localized in τ to the vicinity of the laser pulse and reaches a maximum of ~ 18 kW/cm² at midpulse ($\tau = \tau_L/2$). In the radial direction, the axial flux extends many plasma wavelength beyond the plasma column.

The EMP power propagating in the axial direction resides outside of the plasma filament and is given by

$$P_{EMP}(\tau) = \frac{c}{4\pi} \int_{r_P}^\infty B_\theta^2(r,\tau) 2\pi\, r dr = \frac{c}{16} B_o^2\, r_p^2 \Lambda(\tau,\tau_L), \quad (41)$$

where $\Lambda(\tau,\tau_L) = \ln[(1+\hat{\tau}^2)(1+\Delta\hat{\tau}^2)] - 2\ \mathrm{sgn}\,[\hat{\tau}\Delta\hat{\tau}] \times \ln[C(\hat{\tau},\hat{\tau}_L)]$,
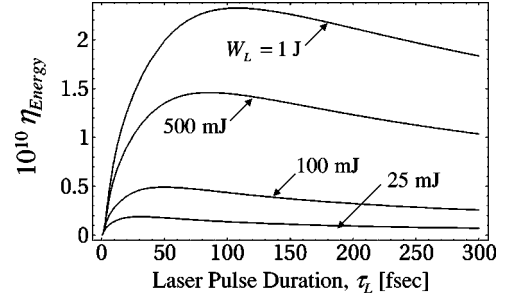

FIG. 2. Steady state EMP conversion efficiency given by Eq. (43) vs laser pulse duration for various laser pulse energies.

$$C(\hat{\tau},\hat{\tau}_L)$$
$$= \frac{2\hat{\tau}^2\,\Delta\hat{\tau}^2 + \hat{\tau}^2 + \Delta\hat{\tau}^2 + 2|\hat{\tau}||\Delta\hat{\tau}|(\hat{\tau}^2\,\Delta\hat{\tau}^2 + \hat{\tau}^2 + \Delta\hat{\tau}^2 + 1)^{1/2}}{\hat{\tau}^2 + \Delta\hat{\tau}^2 + 2|\hat{\tau}||\Delta\hat{\tau}|},$$

$$\hat{\tau} = v_g\, \gamma_g\tau/r_p,$$

$\hat{\tau}_L = v_g\, \gamma_g\tau_L/r_p$, and $\Delta\hat{\tau} = \hat{\tau} - \hat{\tau}_L$. The power ratio, $P_{EMP}(\tau)$ normalized to the peak laser power P_L, is typically very small, with a peak value of $\sim 4 \times 10^{-10}$ for the parameters listed above.

The energy in the EMP pulse is

$$W_{EMP} = \int_{-\infty}^\infty d\tau P_{EMP}(\tau) = \frac{c}{16} B_o^2\, r_p^2 \int_{-\infty}^\infty d\tau \Lambda(\tau,\tau_L). \quad (42)$$

The energy efficiency, defined as the ratio of the EMP energy to the laser energy, is given by

$$\eta_{energy} = \frac{W_{EMP}}{W_L} = \frac{\lambda_o^2 I_L}{8\pi\, P_o} \left(\frac{r_p\omega_{po}}{R_o\omega_o} \right)^2 \Psi(\hat{\tau}_L), \quad (43)$$

where $P_o = m^2c^5/q^2 = 8.75$ GW,

$$\Psi(\hat{\tau}_L) \equiv \tau_L^{-1} \int_{-\infty}^\infty d\tau\, \Lambda(\tau,\tau_L), \quad (44)$$

and the laser pulse energy is $W_L = (c/16)|\hat{E}_L|^2 R_o^2 \tau_L$. The EMP conversion efficiency, Eq. (43), is plotted in Fig. 2. For typical laser parameters the efficiency is extremely small, $\eta_{energy} \approx 4 \times 10^{-10}$.

3. EMP in the transient regime

In this section EMP generation for nonsteady state, i.e., transient, pulse propagation is discussed. To understand radiative EMP we employ a heuristic model in which the nonsteady state regime is represented by a spatially periodic density variation in the pulse propagation direction arising, for example, from the periodic focusing and defocusing of the laser pulse. This variation is also manifested in the components of the laser field within the filament. Since all the field components can be expressed in terms of the axial electric field we spatially modulate this axial field by the factor $[1 + \varepsilon\cos(K z)]$, where $K > 0$ is the wave number associated with the nonsteady state component of the ponderomotive force and ε is a measure of the modulation. In the spatially

modulated medium the ponderomotive force has superluminal Fourier components for a range of K. For these values of K the EMP is radiative, resulting in net power flow in the radial direction. This can be understood by noting that the Fourier transform of the axial electric field outside of the filament is given by [see Eqs. (23)]

$$\left[\frac{1}{r} \frac{\partial}{\partial r} \left(r \frac{\partial}{\partial r} \right) - \kappa_\pm^2 (\omega, K) \right] \tilde{E}_z (\omega, K) = 0, \qquad (45)$$

where

$$\kappa_\pm^2 (\omega, K) = \kappa_o^2 (\omega, \pm K) = \frac{\omega^2}{v_g^2 \gamma_g^2} \pm 2 \frac{\omega}{v_g} K + K^2$$

$$= \left(\frac{\omega}{v_g} \pm K \right)^2 - \frac{\omega^2}{c^2}. \qquad (46)$$

Following Fourier inversion the solutions of Eq. (45) are expressible in the form $K_o(\kappa_\pm r) \exp(\pm i K z) \exp(-i \omega \tau)$. These solutions represent the radial variation of the forward propagating, $\exp(iK z)$, and the backward propagating, $\exp(-iK z)$, contributions to the EMP, respectively, where the transverse wave number is $\kappa_\pm$.

For the purpose of discussing the nature of the solutions, i.e., radiative and nonradiative EMP, we consider the limit of zero collision frequency, $\nu_e = 0$. For $\kappa_\pm^2 > 0$ the solution of Eq. (45) represents exponentially decaying nonradiative solutions, i.e., $K_0(|\kappa_\pm|r) \sim r^{-1/2} \exp(-|\kappa_\pm|r)$. Note that the exponentially increasing solution is nonphysical. Since ω and K have been chosen to be positive, κ_+ is always positive and represents exponentially decaying solutions that are nonradiative. However, κ_-^2 can be less than zero for values of K in the range

$$\frac{2 \omega}{c} > K > \frac{\omega}{2 c \gamma_g^2}. \qquad (47)$$

In this case $\kappa_- = \pm i |\kappa_-|$ and the solution $K_o(\kappa_- r)$ for large r represents radiative solutions, i.e., $K_0(\kappa_- r) \sim r^{-1/2} \exp(\mp i |\kappa_-|r)$. Here, the upper sign represents a radially incoming wave and is not physical. The lower sign, however, represents a radially outgoing EMP field and corresponds to radiative fields. The source of the radiative field is the ponderomotive force containing Fourier components with phase velocities that are superluminal. In the laser pulse frame, the Cherenkov-like emission angle of the EMP radiation with respect to the laser pulse propagation direction is

$$\Theta_c = \tan^{-1}(|\kappa_-|/K). \qquad (48)$$

The phase velocity associated with the Fourier components of the ponderomotive force is given by

$$v_{ph} = \frac{\omega v_g}{\omega - v_g K}, \qquad (49)$$

and the EMP is radiative when $v_{ph} > v_g$. The radiative and nonradiative branches of the EMP can be illustrated with a dispersion diagram shown in Fig. 3. The frequency and wave number of the EMP are given by the intersection of the elec-
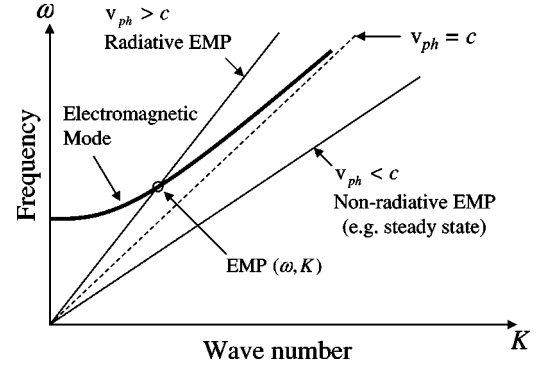

FIG. 3. Dispersion diagram showing the condition for radiative EMP.

tromagnetic mode and the $v_{ph} > c$ dispersion line.

III. EMP GENERATION ON THE SURFACE OF A DIELECTRIC

In this section we analyze the generation of EMP from dielectric surfaces. The incident laser pulse ionizes the dielectric and produces an oscillating plasma current sheet which is a source of EMP. In addition, we assume that the dielectric may have a nonvanishing second-order susceptibility χ_2; this is the case in crystalline dielectrics. A second-order susceptibility can result in optical rectification and be a source of EMP radiation [43]. Other methods for generating THz radiation in solids are discussed in, for example, Refs. [22–25,44].

In previous sections we found the efficiency of laser energy conversion into EMP energy in air to be extremely small. In this section we consider the EMP generated when a laser pulse is incident on a dielectric target. A difference between a dielectric and the atmosphere is that the electron-neutral collision frequency is nearly four orders of magnitude larger in dielectrics. Another difference between a dielectric and the atmosphere is related to the ionization process. Typically, to elevate (ionize) an electron from the valence band into the conduction band in a dielectric requires an amount of energy on the order of a few electron volts. Thus for a laser wavelength of $\lambda_o = 0.8$ μm ($\hbar \omega_o = 1.54$ eV) a few photons suffice to induce photoionization. That is, in Eq. (5), $\ell \approx 2$ and hence the plasma filament is no longer limited to a narrow region near the center of the laser pulse, i.e., the filling factor is nearly unity. Finally, due to the short penetration depth into a dielectric [45,46], self-focusing and diffraction of the laser beam are negligible and consequently a one-dimensional analysis of the EMP generation suffices. The wave equation for the EMP field inside the dielectric is

$$\mathbf{\nabla} \times (\mathbf{\nabla} \times \mathbf{E}) + \frac{n_o^2}{c^2} \frac{\partial^2 \mathbf{E}}{\partial t^2} = -\frac{4\pi}{c^2} \frac{\partial \mathbf{J}}{\partial t} - \frac{4\pi}{c^2} \frac{\partial^2 \mathbf{P}_2}{\partial t^2}, \quad (50)$$

where n_o is the linear index of the dielectric, the plasma current density $\mathbf{J}$ is given by Eq. (6), $\mathbf{P}_2 = \chi_2 |\hat{E}_L|^2 \hat{\mathbf{e}}_x / 2$ is the second-order polarization field polarized in the x direction, χ_2 is the second-order susceptibility, and $\hat{E}_L(z,t)$ is the am-

plitude of the laser pulse inside the dielectric [41,43]. In writing the second-order polarization field, second-harmonic terms have been neglected. A typical value for the second-order susceptibility in crystalline dielectrics is χ_2 $\sim 10^{-7}$ esu. On the right-hand side of Eq. (50), the ratio of the second-order polarization field source term to the radial and axial components of the plasma current density source term are, respectively,

$$\left|(\partial \mathbf{P}_2/\partial t)/\mathbf{J}\cdot\hat{\mathbf{e}}_r\right| \sim 4\,\pi\frac{m\,c}{q}\frac{\omega_o^2}{\omega_p^2}\frac{\chi_2}{\tau_L}\left(\frac{2\,\nu_e R_o}{c}\right), \quad (51a)$$

$$\left|(\partial \mathbf{P}_2/\partial t)/\mathbf{J}\cdot\hat{\mathbf{e}}_z\right| \sim 4\,\pi\frac{mc}{q}\frac{\omega_o^2}{\omega_p^2}\frac{\chi_2}{\tau_L}. \quad (51b)$$

In obtaining Eqs. (51) it was assumed that the process is in the collisionally dominant regime, $\nu_e\,\tau_L\gg 1$. For ω_o/ω_p ~ 10, $\tau_L\sim 100$ fsec, $\nu_e\sim 10^{16}$ sec^{-1}, and spot size of R_o ~ 200 μm the ratios in Eqs. (51a) and (51b) are $\sim 10^6$ and 10^2, respectively. This indicates that the optical rectification process, compared to the plasma generation process, can be a far more efficient mechanism for generating EMP in crystalline materials.

The interaction of a laser pulse with a dielectric surface can lead to significant heating of electrons provided that the pulse duration is long compared with the electron collision time. The hot electrons radiate part of their energy in the form of bremsstrahlung covering a broad spectrum. As an example, consider a 100 fsec duration, 0.8 μm wavelength laser pulse with intensity 10^{13} W/cm^2 propagating in a singly ionized plasma with electron density 2×10^{21} cm^{-3} and collision frequency 10^{16} sec^{-1}. The characteristic bremsstrahlung energy in this case is ~ 150 eV (soft x-ray regime) and the energy conversion efficiency is $\sim 10^{-4}$. The inclusion of line radiation and recombination radiation can increase this efficiency by factors of order unity.

To obtain both the current density and second-order polarization field on the right-hand side of Eq. (50), the laser pulse amplitude $\hat{E}_L$ is required. To obtain the laser pulse amplitude we write the incident, reflected, and transmitted laser pulse fields as follows:

$$\mathbf{E}_{in}(z,t) = (1/2)E_{in}(t-z/c)\exp[i(k_o z-\omega_o t)]\hat{\mathbf{e}}_x + \text{c.c.}, \quad (52a)$$

$$\mathbf{E}_R(z,t) = (1/2)E_R(t+z/c)\exp[-i(k_o z+\omega_o t)]\hat{\mathbf{e}}_x + \text{c.c.}, \quad (52b)$$

$$\mathbf{E}_L(z,t) = (1/2)\hat{E}_L(z,t)\exp(-i\omega_o t)\hat{\mathbf{e}}_x + \text{c.c.}, \quad (52c)$$

where $k_o=\omega_o/c$ in the vacuum region. The laser field inside the dielectric satisfies

$$\frac{\partial^2 \mathbf{E}_L}{\partial z^2} - \frac{1}{c^2}\frac{\partial^2 \mathbf{E}_L}{\partial t^2} = \frac{4\pi}{c^2}\frac{\partial \mathbf{J}_L}{\partial t} + \frac{4\pi}{c^2}\frac{\partial^2 \mathbf{P}}{\partial t^2}, \quad (53)$$

where $\mathbf{J}_L(z,t)$ and $\mathbf{P}(z,t)$ are, respectively, the current density and total polarization fields. Within the dielectric the current density is given by Eq. (2), where

$$\mathbf{J}_L(z,t) = (1/2)\hat{J}_L(z,t)\exp(-i\,\omega_o t)\hat{\mathbf{e}}_x + \text{c.c.} \quad (54)$$

is the laser driven plasma current density. The rate of change of plasma density is given by Eq. (4a). The polarization field consists of a linear and a nonlinear contribution,

$$\mathbf{P}(z,t) = (1/2)[P_L(z,t)+P_{NL}(z,t)]\exp(-i\,\omega_o t)\hat{\mathbf{e}}_x + \text{c.c.}, \quad (55)$$

where $\hat{P}_L(z,t)=\chi_L\hat{E}_L(z,t)$, $\hat{P}_{NL}=\alpha|\hat{E}_L(z,t)|^2\hat{E}_L(z,t)$, χ_L is the linear susceptibility, and α is related to the nonlinear Kerr refractive index. Note that the second-order polarization field in Eq. (55) is omitted since it does not contribute to a driving term at the laser frequency. If the laser pulse duration is long compared to the laser period, i.e., $\omega_o\gg|\partial/\partial t|$, Eqs. (53) and (2) can be written as

$$\left[\frac{\partial^2}{\partial z^2} + \frac{\omega_o^2 n_o^2}{c^2}\left(1+\frac{2i}{\omega_o}\frac{\partial}{\partial t}\right)\right]\hat{E}_L(z,t)$$
$$= -\frac{4\pi i}{c^2}\omega_o\left(1+\frac{i}{\omega_o}\frac{\partial}{\partial t}\right)\hat{J}_L(z,t) - \frac{4\pi\omega_o^2}{c^2}\alpha|\hat{E}_L|^2\hat{E}_L(z,t), \quad (56a)$$

$$\left(1+\frac{i}{(\omega_o+i\nu_e)}\frac{\partial}{\partial t}\right)\hat{J}_L(z,t) = \frac{i}{4\pi(\omega_o+i\nu_e)}\omega_p^2(z,t)\hat{E}_L(z,t), \quad (56b)$$

where $n_o=(1+4\pi\chi_L)^{1/2}$ is the linear refractive index. To lowest order in $\partial/\partial t$, Eqs. (56a) and (56b) combine to give

$$\left[\frac{\partial^2}{\partial z^2} + K^2(z,t) + 2i\frac{\omega_o}{c^2}\left(n_o^2-\frac{i}{2}\frac{\nu_e}{\omega_o}\frac{\omega_p^2(z,t)}{(\omega_o+i\nu_e)^2}\right)\frac{\partial}{\partial t}\right]\hat{E}_L(z,t)$$
$$= 0, \quad (57)$$

where

$$K(z,t) = \frac{\omega_o}{c}\left(n_o^2 - \frac{\omega_p^2(z,t)}{\omega_o(\omega_o+i\nu_e)} + 4\pi\alpha|\hat{E}_L(z,t)|^2\right.$$
$$\left. + \frac{\nu_e/\omega_o^2}{(\omega_o+i\nu_e)^2}\frac{\partial\,\omega_p^2(z,t)}{\partial t}\right)^{1/2}, \quad (58a)$$

$$\frac{\partial\,\omega_p^2(z,t)}{\partial t} = \frac{2\pi\omega_n^2\omega_o}{(\ell-1)!}\left(\frac{I_L(z,t)}{I_{MP}}\right)^\ell, \quad (58b)$$

and $\omega_n=(4\pi\,q^2 n_{no}/m)^{1/2}\sim 1.8\times 10^{16}$ sec^{-1} for n_{no} $\sim 10^{23}$ cm^{-3}. Note that $4\pi\alpha|\hat{E}_L(z,t)|^2=2n_o n_K(n_n/n_{no})I_L(z,t)$, where n_K is the nonlinear Kerr refractive index, $n_n=n_{no}-n_e$, and $I_L(z,t)=cn_o|\hat{E}_L(z,t)|^2/8\pi$ is the laser pulse intensity. For a dielectric the number of photons needed for ionization is
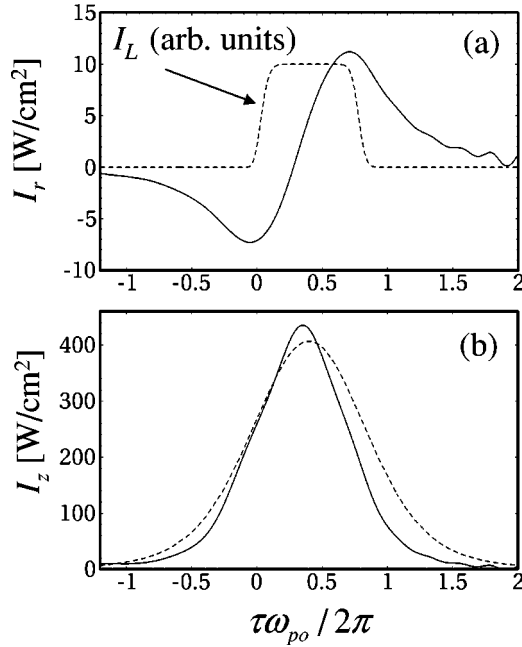
FIG. 4. EMP radiance vs normalized τ at radial position $r = 70\ c/\omega_{po}$ (outside the plasma filament). Laser parameters are $\lambda_o = 0.8\ \mu$m, $\tau_L = 267$ fsec, $\gamma_g = 13$, and peak laser intensity $I_{L0} = 7 \times 10^{13}$ W/cm². Plasma parameters are $n_{eo} = 1.1 \times 10^{17}$ cm⁻³ and $r_p = 0.4$ mm. Panel (a) shows the steady state radial EMP radiance, $I_r = cE_z B_\theta / 4\pi$ (solid curve), and the laser intensity profile I_L (dashed curve). Panel (b) shows the corresponding axial EMP radiance I_z (solid curve) from the simulation and the analytical calculation of $I_z = cB_\theta^2 / 4\pi$ (dashed curve) for steady state propagation where B_θ is obtained from Eq. (39).

typically small, i.e., $\ell = 1$, 2, or 3 , $\lambda_o = 0.8\ \mu$m. Equation (57) together with Eqs. (58) describe the evolution of a laser pulse propagating in an ionizing dielectric. In dielectrics collisional and ionization absorption of the laser pulse takes place over a short distance, i.e., the penetration depth is a few microns. For distances short compared to the laser pulse length, i.e., $z \ll c\tau_L / n_o$, transit time effects can be neglected. In this limit $\partial / \partial t$ can be neglected and Eq. (57) reduces to

$$\left(\frac{\partial^2}{\partial z^2} + K^2(z,t) \right) \hat{E}_L(z,t) = 0. \tag{59}$$

The WKB solution of Eq. (59) is

$$\hat{E}_L(z,t) = \hat{E}_L(0,t) \left(\frac{K(0,t)}{K(z,t)} \right)^{1/2} \exp\left(i \int_0^z dz'\ K(z',t) \right), \tag{60}$$

where solutions representing waves traveling towards the left are not considered. The value of the field at the boundary, i.e., $\hat{E}_L(0,t)$, is obtained from the boundary conditions. Applying the boundary conditions at $z=0$ yields

$$E_{in}(t) + E_R(t) = \hat{E}_L(0,t)$$

and

$$E_{in}(t) - E_R(t) = \hat{E}_L(0,t)\{K(0,t) + (i/2)[\partial \ln(K)/\partial z]_{z=0}\}/k_o,$$

which combine to give

$$\hat{E}_L(0,t) = \frac{2\ k_o\ E_{in}(t)}{k_o + K(0,t) + \dfrac{i}{2}\left(\dfrac{\partial \ln(K)}{\partial z} \right)_{z=0}}. \tag{61}$$

Within the dielectric the laser pulse amplitude is given by Eq. (60) together with Eq. (61). The laser pulse amplitude determines the current density given by Eq. (2) and the second-order polarization field which drives the EMP fields in Eq. (50). These equations are solved numerically in Sec. IV.

IV. NUMERICAL SIMULATIONS OF EMP GENERATION

The numerical simulations presented in this section are based on solving Eq. (20) for the EMP field, with the plasma current and source given by Eqs. (6), (8), and (10). The laser envelope evolves according to Eqs. (14) and the ionization generated plasma density is given by Eq. (15c). The characteristic ionization and recombination parameters used in the simulations are discussed following Eq. (5). The system of equations is solved in axisymmetric cylindrical geometry and evolved using a time and space centered finite differencing scheme with the electric field and plasma density calculated on the same grid and the magnetic field and plasma current calculated on a separate, staggered grid. The equations for the EMP fields are solved in the laboratory frame characterized by the variables (r,z,t). The propagation equations for the driving laser pulse are solved in the group velocity frame and transformed to the laboratory frame when coupled to the EMP equations.

The SDE method [42] of solving for the laser pulse amplitude provides a description of the laser pulse evolution that is simple to implement numerically. However, it is based on the premise that the transverse laser profile is approximately Gaussian. In certain regimes this may be violated as, for example, in Fig. 13 of Ref. [36], where a hollowing of the laser pulse takes place. In such cases, the solution of Eq. (11) must be employed. In the following we shall assume that the Gaussian profile approximation is valid.

The simulations are initialized at $t=0$ with the laser pulse propagating in vacuum in the positive z direction. The leading edge of the laser pulse at $t=0$ is located at axial position $z=0$. This configuration provides the initial condition for the numerical EMP field solver, namely, that the initial EMP fields are zero. In the vacuum-air transition region from $z=0$ to $z=L_n$, the neutral density increases with the functional form

$$n_n(z) = n_{no} \begin{cases} 1, z \geqslant L_n \\ [10(z/L_n)^3 - 15(z/L_n)^4 + 6(z/L_n)^5], & 0 \leqslant z \leqslant L_n \end{cases}, \tag{62}$$

and has the constant value $n_{no} = 2.7 \times 10^{19}$ cm⁻³ for $z > L_n$. The chosen z dependence of the neutral density assures that the first and second z derivatives of the density are continuous at $z=0$ and $z=L_n$.
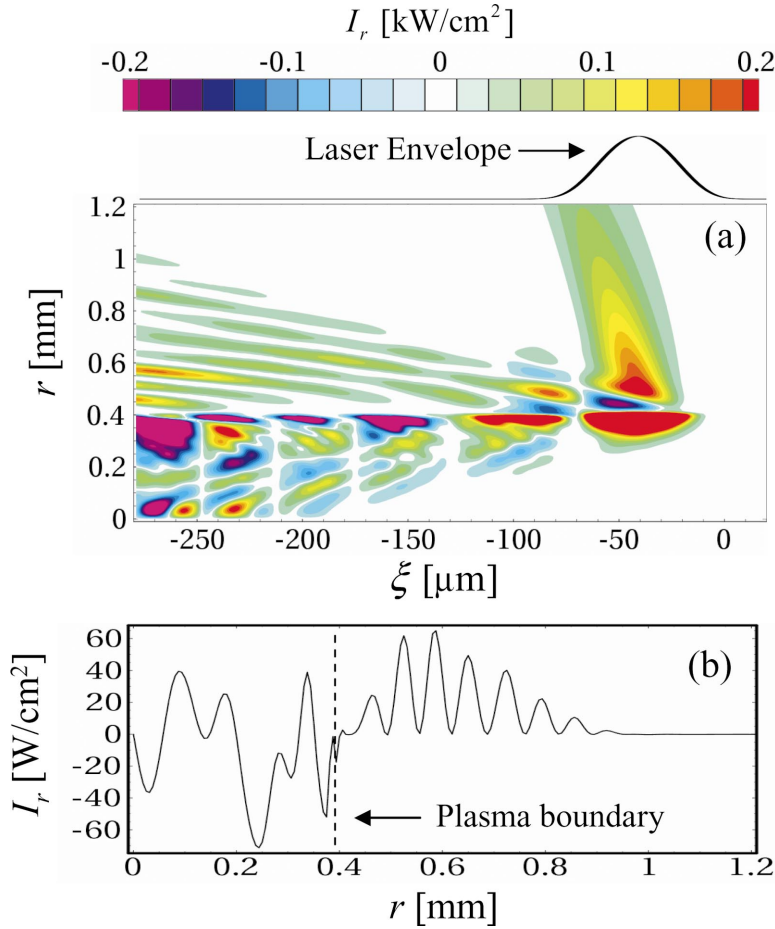
FIG. 5. (Color) (a) Shaded contours of radial power flux I_r as a function of $\xi = z - v_g t$ and radial position r showing radiative EMP from a modulated plasma filament with plasma density $n_{eo} = 1.1 \times 10^{17}$ cm^{-3} and radius $r_p = 0.4$ mm. (b) I_r vs radial position at axial position $\xi = -220$ μm. The plasma modulation is characterized by amplitude $\varepsilon = 0.3$ and wave number $K = \omega_p / 4\,c$ as defined by Eq. (47). Laser parameters are $\lambda = 0.8$ μm, $I_{L0} = 7 \times 10^{13}$ W/cm^2, $\tau_L = 267$ fsec, and $\gamma_g = 109$.

A. EMP generation in air

The following four examples illustrate the generation of EMP from the interaction of an ultrashort laser pulse with air. The first two examples validate the numerical simulation with the analyses of Sec. III. The third example is a simulation of a recent experiment which observed EMP emitted from a laser pulse propagating in air. The last example in this section shows EMP generation from a much higher intensity laser pulse which fully ionizes the air.

1. Steady state laser pulse propagation

This first example benchmarks the numerical simulation with the steady state analysis of Sec. III. A laser pulse propagates through a preformed plasma filament characterized by a constant density $n_e = 10^{17}$ cm^{-3} ($\omega_{po} = 1.9 \times 10^{13}$ sec^{-1}) in the region $r < r_p$ and $n_e = 0$ for $r > r_p$, where the filament radius is $r_p = 0.4$ mm ($\sim 25 c/\omega_{po}$). The laser spot size is assumed to be much larger than r_p so that the transverse variation of the laser envelope can be neglected. To approximate the square laser pulse profile assumed in the analysis, the laser envelope in the simulation is taken to have a longitudinal profile given by $E_L(\tau) = E_{L0} \sin^2[\pi(\tau/\tau_L)^{16}/2]$ for $0 < \tau < \tau_L$ and $E_L(\tau) = 0$ otherwise. The smooth variation of the laser envelope at the leading and trailing edges reduces numerical dispersion. The pulse duration, $\tau_L = 270$ fsec $\sim 0.8 \times 2\pi/\omega_{po}$, is chosen to optimally excite a plasma wave under collisionless conditions. The peak laser intensity is

$I_{L0} = 7 \times 10^{13}$ W/cm^2 and the laser wavelength is $\lambda_o = 0.8$ μm. To be consistent with the steady state analysis, the laser envelope is independent of the propagation distance η and the radial EMP source term given by Eq. (10) is neglected in this simulation example.

The length of the vacuum-air transition region for this simulation example is $L_n = 20\,c/\omega_{po} = 0.3$ mm. A transient EMP is generated in this transition region which must be allowed to propagate away from the laser pulse before the steady state is achieved. To achieve steady state, the laser pulse must propagate a distance $z \gg 2\gamma_g^2 c \tau_L$. To reduce computer run time and expedite reaching the steady state, a
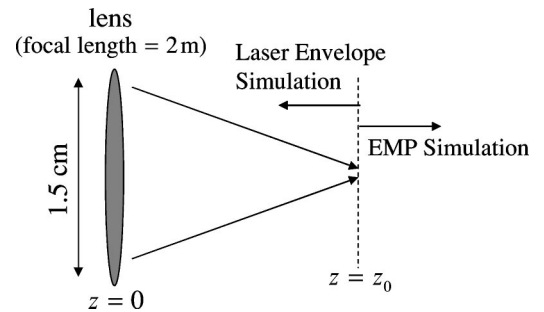

FIG. 6. Schematic diagram of the simulation of the EMP experiment of Ref. [17]. The laser envelope simulation (without EMP) is performed from $z = 0$ to $z = z_0$, where $z_o = 1.82$ m. The full EMP simulation is carried out for $z > z_o$.
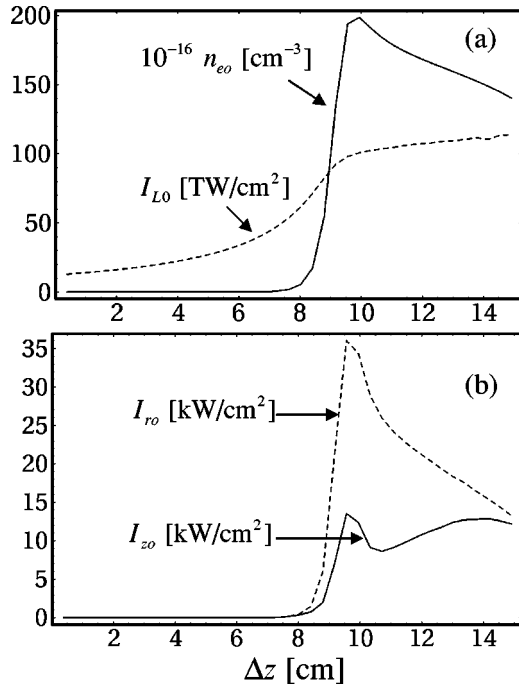
FIG. 7. (a) Peak plasma density and laser intensity vs propagation distance $\Delta z = z - z_o$ for the simulation of the experiment of Ref. [17]. (b) Peak radial (dashed curve) and axial (solid curve) Poynting flux vs Δz. Initial ($z=0$) laser parameters for the simulation are $\lambda_o = 0.8$ μm, $P_L = 83$ GW, $\tau_L = 120$ fsec (FWHM), and $R_o = 7.5$ mm. Parameters for air are taken to be $n_o - 1 = 2.7 \times 10^{-4}$, $n_K = 3 \times 10^{-19}$ cm^2/W, $U_{ion} = 12$ eV, $\ell = 8$, and $I_{MP} \sim 10^{14}$ W/cm^2.

FIG. 8. (a) Normalized on-axis laser intensity vs time, (b) radial EMP Poynting flux I_r at radial position $r = 225$ μm vs time, and (c) corresponding temporal Fourier transform of I_r for propagation distances $\Delta z = 10$ cm (dashed curve) and 12 cm (solid curve). The radial position $r = 225$ μm is outside of the plasma filament. Simulation parameters correspond to those listed for Fig. 7.

vacuum ($n_o = 1$) is assumed outside of the plasma filament and the laser pulse is given an artificially low group velocity, $\gamma_g = 13$. For these parameters, the minimum propagation distance required to reach steady state is ~ 3 cm.

The radial EMP Poynting flux $I_r = c \ E_z B_\theta / 4\pi$ (solid curve) and laser intensity profile (dashed curve) outside the plasma filament is plotted in Fig. 4(a) as a function of normalized time $\tau \omega_{po}/2\pi$. Note the adjacent regions of positive and negative radial flux which, when integrated over time, nearly cancel. This result is consistent with the analytical prediction that the EMP field is nonradiative in the steady state and there is no net radial energy flux. Figure 4(b) shows that there is, however, a much larger net axial Poynting flux ($I_z = c B_\theta^2 / 4\pi \sim 400$ W/cm^2) in the simulation which is in agreement with the analysis. The axial EMP flux is localized longitudinally roughly within the laser pulse.

2. Transient laser pulse propagation

In the next example, we verify the condition for radiative EMP given by Eq. (47). A laser pulse with longitudinal profile given by $E_L(\tau) = E_{L0}\sin[\pi\tau/\tau_L]$ for $0 < \tau < \tau_L$ and $E_L(\tau) = 0$ otherwise, pulse duration $\tau_L = 270$ fsec $\sim 0.8 \times \pi/\omega_{po}$, peak laser intensity $I_{L0} = 7 \times 10^{13}$ W/cm^2, and wavelength $\lambda_o = 0.8$ μm propagates through a modulated, preformed plasma filament. The plasma density is given by $n_e(r,z) = n_{eo}[1 - \Theta(r - r_p)][1 + \varepsilon \sin(Kz)]$, where $n_{eo} = 10^{17}$ cm^{-3}, the modulation amplitude is $\varepsilon = 0.3$, and $\Theta(x)$ is the Heaviside

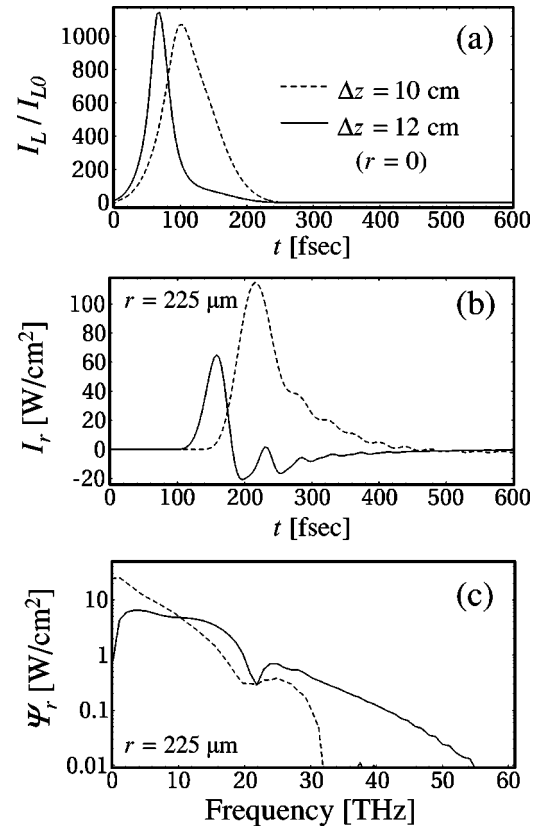unit step function. As in the previous example, there is a transition region from vacuum to air with a scale length $L_n = 20c/\omega_{po} = 0.3$ mm. The linear and nonlinear (Kerr) indices of air are chosen to be $n_o - 1 = 2.7 \times 10^{-4}$ and $n_K = 6 \times 10^{-19}$ cm^2/W, respectively. For these parameters, the relativistic factor associated with the laser group velocity [see Eq. (22)] has the value $\gamma_g = 109$. The laser envelope is taken to be independent of the propagation distance η and the radial EMP source term given by Eq. (10) is neglected to be consistent with the analysis. Note that for an unmodulated plasma filament, the distance required to reach steady state for these parameters is ~ 2 m.

Figure 5 shows the spatial EMP distribution generated from a modulated plasma filament. The modulation wave number, $K = \omega_{po}/4c$, is chosen to satisfy the condition for radiative EMP given by Eq. (47) assuming that the characteristic frequency $\omega \sim \omega_{po}$. Figure 5(a) plots the spatial ($\xi = z - v_g t, r$) distribution of the radial Poynting flux I_r after a propagation distance of ~ 2 cm. Radiative EMP is observed propagating from the plasma channel behind the laser pulse. The radiation is confined to a cone characterized by the Cherenkov angle given by Eq. (48). The outward EMP flux observed within the laser pulse (-80 μm $< \xi < 0$) is a manifestation of the transient interaction at the vacuum-air transition region. It is expected that there would be no net out-
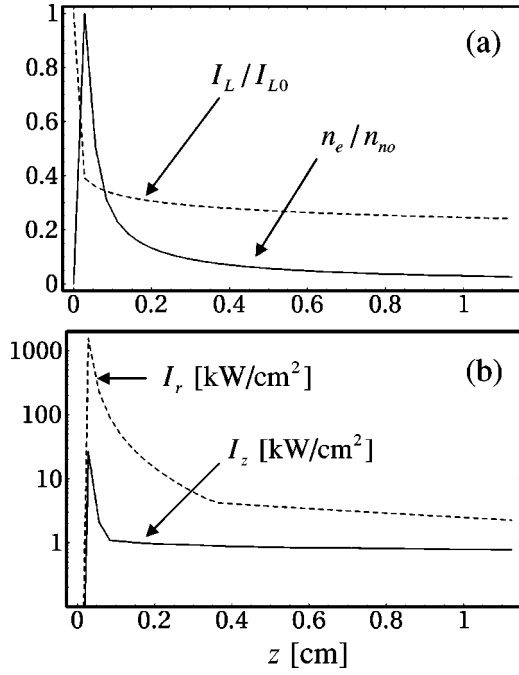
FIG. 9. (a) Normalized peak laser intensity I_L/I_{L0} (dashed curve) and normalized peak plasma density n_e/n_{no} as a function of propagation distance for an initially collimated laser pulse with $\lambda_o = 0.8$ μm, $P_L = 5.3$ TW, $\tau_L = 240$ fsec, and $R_o = 1$ mm. Parameters for air are taken to be $n_o - 1 = 2.7 \times 10^{-4}$, $n_K = 3 \times 10^{-19}$ cm^2/W, $U_{ion} = 12$ eV, $\ell = 8$, and $I_{MP} = 10^{14}$ W/cm^2. (b) Corresponding peak radial (dashed curve) and axial (solid curve) Poynting flux as a function of propagation distance.

ward flux in the region -80 μm $< \xi < 0$ had the simulation reached the steady state regime after 2 m of propagation. In Fig. 5(b), the radial profile of I_r behind the laser pulse at axial position $\xi = -220$ μm shows an outward Poynting flux on the order of 100 W/cm^2 extending outside the plasma filament. Consistent with the analysis, for simulation parameters identical to those of Fig. 5, except that the modulation wave number, $K = 4$ ω_{po}/c, we find an absence of radial flux behind the laser pulse outside the plasma filament.

3. Simulation of experiment

A recent experiment at the Applied Optics Laboratory (LOA) reported in Ref. [17] measured an EMP from a femtosecond laser pulse propagating in air. In the experiment, a laser pulse with a FWHM (full width at half maximum) duration of 120 fsec, wavelength $\lambda_o = 0.8$ μm, and energy ~ 30 mJ was passed through an aperture of diameter 1.5 cm and focused into the air with a 2 m focal length lens. As the laser pulse focused and the intensity increased, a plasma filament was formed near the focal region and EMP was measured along the length of the plasma filament. The following results are from a simulation with similar parameters. A detailed comparison with the experiment is beyond the scope of this paper due to uncertainties in the measurements. However, the simulations do reveal a number of features that are difficult to diagnose in experiments.

In our simulation, the parameters for air are taken to be $n_o - 1 = 2.7 \times 10^{-4}$, $n_K = 3 \times 10^{-19}$ cm^2/W, $U_{ion} = 12$ eV, $\ell = 8$,

$I_{MP} = 10^{14}$ W/cm^2, and $n_{no} = 2.7 \times 10^{19}$ cm^{-3}. The laser pulse envelope is taken to be Gaussian in the transverse direction with a spot size $R_o = 7.5$ mm. The longitudinal laser field profile is given by Eq. (25) with $\tau_L = 240$ fsec, which corresponds to a FWHM intensity duration of 120 fsec. The laser pulse has wavelength $\lambda_o = 0.8$ μm, peak power $P_L = 83$ GW, and energy ~ 10 mJ. The simulation is performed in two parts as illustrated in Fig. 6. The first part models the focusing of the initially low intensity laser pulse in air by a lens with a focal length of 2 m. Here the simulation covers a range $0 < z < z_o$, where $z_o = 1.82$ m. Over this range, the laser intensity is sufficiently low that no appreciable plasma density is formed and no EMP is generated. To expedite the simulation, only the propagation equations for the driving laser pulse envelope are solved for $z < z_o$. The laser pulse envelope at $z = z_o$ is used to initialize the full-scale EMP simulation for $z > z_o$.

Figure 7(a) plots the peak plasma density (solid curve) and laser intensity (dashed curve) over the range $0 < \Delta z < 16$ cm, where $\Delta z = z - z_o$ is the distance from the start of the full-scale EMP simulation. For $\Delta z < 9$ cm, the laser intensity increases due to both geometric and nonlinear focusing. For $\Delta z > 9$ cm, a plasma filament is formed on axis which defocuses the trailing edge of the laser pulse, thereby resulting in a shorter duration laser pulse. The peak plasma density achieved in the simulation is $\sim 2 \times 10^{18}$ cm^{-3}, which occurs at $\Delta z \sim 10$ cm. For $\Delta z > 10$ cm the plasma density steadily decreases due to the shortening of the laser pulse. Figure 7(b) plots the corresponding peak values of the axial (solid curve) and radial (dashed curve) Poynting fluxes as a function of Δz. The maximum EMP flux coincides with the maximum plasma density. The maximum radial flux is $I_r \sim 35$ kW/cm^2 while the maximum axial flux is $I_z \sim 15$ kW/cm^2. Significant shortening of the driving laser pulse prevented the simulation from extending beyond $\Delta z \sim 16$ cm without violating the assumption that group velocity dispersion is negligible.

Figure 8(a) plots the on axis laser intensity (normalized to its peak value at $z = 0$) versus time at $\Delta z = 10$ cm (dashed curve) and $\Delta z = 12$ cm (solid curve). The relatively shorter pulse duration at $\Delta z = 12$ cm is the result of plasma defocusing of the trailing edge of the laser. Figure 8(b) plots the corresponding radial Poynting flux versus time at radial position $r = 225$ μm. The Poynting flux is peaked in a region behind the driving laser pulse and has a duration that is of the order $\sim 1/\nu_e$. Note that the flux at $\Delta z = 10$ cm is directed radially outward while at $\Delta z = 12$ cm, it is outward just behind the laser pulse and then reverses direction. Figure 8(c) plots the frequency distribution of the two curves shown in Fig. 8(b). The frequency distribution

$$\psi_r(r_0, \omega) \equiv \frac{\Delta \omega}{\sqrt{2\pi}} \int_{-\infty}^{\infty} I_r(r_0, t) e^{i\omega t} dt \qquad (63)$$

has units of intensity and represents the intensity contained within a frequency band $\Delta \omega$. In this case, $\Delta \omega / 2\pi \sim 1$ THz is the smallest frequency interval that can be resolved by the simulation grid size. The EMP spectrum at $\Delta z = 10$ cm is peaked near zero frequency and is broadband with a width of
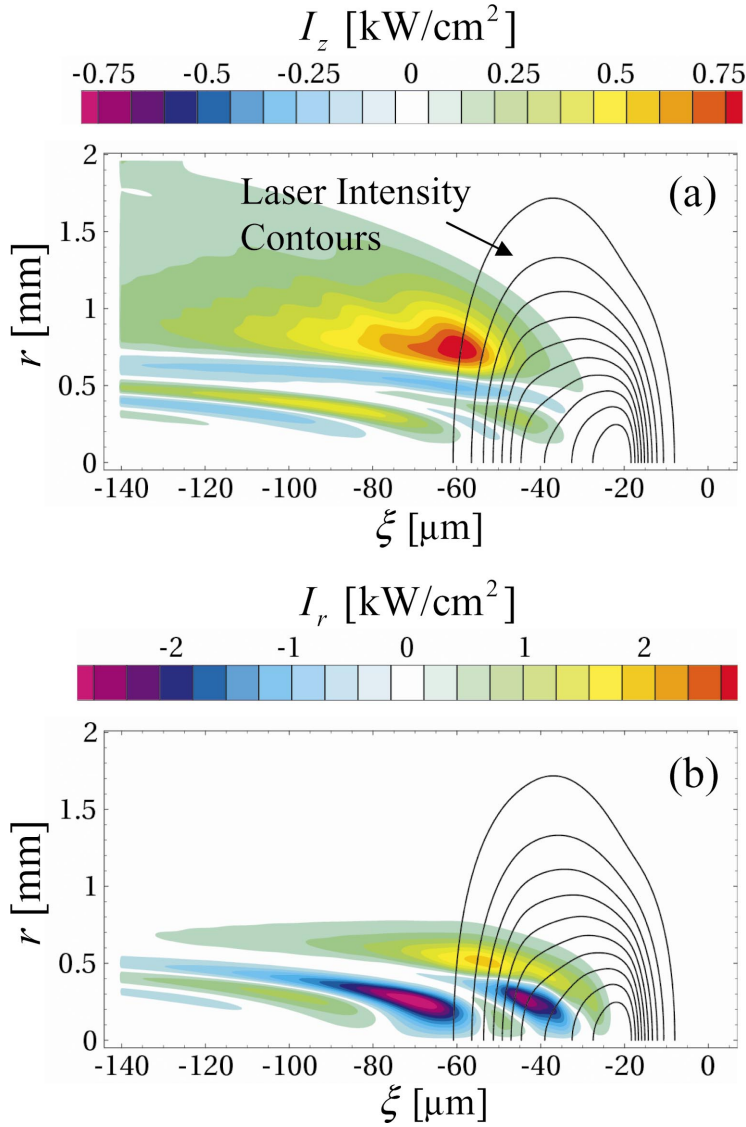
FIG. 10. (Color) Contours of laser intensity (unshaded) and (a) axial and (b) radial Poynting flux (shaded contours) in the (ξ, r) plane at propagation distance $z=0.8$ cm corresponding to the simulation of Fig. 9.

$\sim$10 THz. At $\Delta z=10$ cm, the maximum electron collision frequency $\nu_e \sim 6 \times 10^{13}$ sec^{-1}. At $\Delta z=12$ cm, the spectrum is broader and a local maximum at a frequency of $\sim$2 THz is apparent. The peak plasma frequency varies from $\sim$13 THz to $\sim$12 THz over 2 cm of propagation shown in the plots. Note that there is no distinct feature in the EMP spectrum at the plasma frequency or any of its harmonics.

The total EMP power emitted radially through a cylindrical surface of radius $r_o=580$ μm versus time is given by

$$P_r(t) = 2\pi r_o \int_{-\infty}^{\infty} I_r(r_o, z, t) dz. \qquad (64)$$

In our simulations, we find that the power has a maximum of $\sim$0.8 W. Most of the power is emitted over a duration $\sim$0.1 nsec. Integrating the power over time, the total energy radiated in the radial direction during the entire simulation is found to be $\sim$50 pJ, which corresponds to an energy conversion efficiency of $\sim 5 \times 10^{-9}$.

4. High energy laser pulse

As a final example of atmospheric EMP generation, we consider the propagation of a high-energy ($\sim$1 J), high-intensity ($>10^{14}$ W/cm^2) ultrashort laser pulse in air. In this example, the initial laser pulse is Gaussian in the transverse direction with a spot size $R_o=1$ mm. The longitudinal envelope is given by

$$|E_L(0, z, \tau)| = \hat{E}_L(z)\sin^2(\pi\tau/\tau_L) \qquad (65)$$

for $0 \le \tau \le \tau_L$ and zero otherwise, with $\tau_L=240$ fsec. The laser pulse is initially collimated and has wavelength $\lambda_o = 0.8$ μm, peak power $P_L=5.3$ TW, intensity $I_{L0}=3.5 \times 10^{14}$ W/cm^2, and energy $\sim$0.5 J. Parameters for air are taken to be $n_o - 1 = 2.7 \times 10^{-4}$, $n_K = 3 \times 10^{-19}$ cm^2/W, $U_{ion} = 12$ eV, $\ell = 8$, and $I_{MP}=10^{14}$ W/cm^2. The air-vacuum interface has scale length $\sim$70 μm.

Figure 9(a) shows the normalized peak laser intensity I_L/I_{L0} and normalized peak plasma density n_e/n_{no} as a function of propagation distance. At $z=0$, the laser pulse is in vacuum. As the laser pulse enters the air, the air is fully
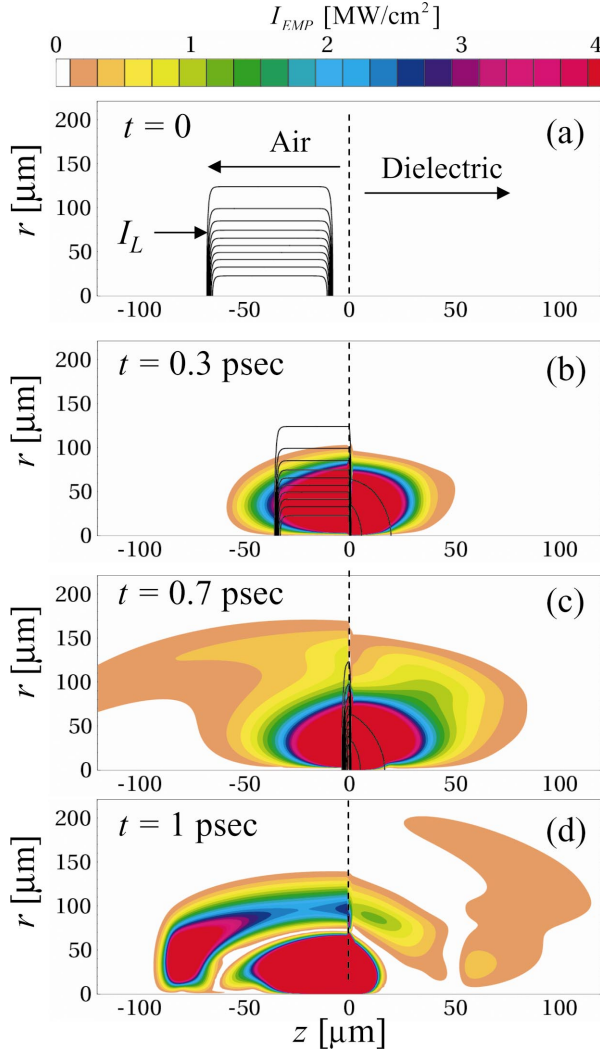
FIG. 11. (Color) Simulation of EMP generation from a dielectric surface. Panels show laser intensity (unshaded contours), and total EMP flux $I_{EMP}=(I_r^2+I_z^2)^{1/2}$ (shaded contours) in the (z,r) plane at times (a) $t=0$, (b) $t=0.3$ psec, (c) $t=0.7$ psec, and (d) $t=1$ psec. Dashed line at $z=0$ indicates the boundary between air $(z<0)$ and dielectric $(z>0)$. Laser parameters at $t=0$ are $\lambda_o=0.8$ μm, $I_{L0}=10^{13}$ W/cm^2, $\tau_L=200$ fsec, and $R_o=0.1$ mm. Parameters for the dielectric are taken to be $n_o=3$, $n_K=7\times10^{-15}$ cm^2/W, $U_{ion}=3$ eV, $\ell=2$, and $I_{MP}=5\times10^{14}$ W/cm^2.

ionized and the laser intensity decreases rapidly. Note that for the initial parameters of the simulation, the scale length for laser energy depletion due to ionization is ~8 μm. Over a propagation distance of ~1 cm, the laser pulse is seen to lose more than $\sim70\%$ of its energy. As the laser intensity decreases, the plasma density is also seen to decrease. The corresponding values of peak radial and axial Poynting flux are plotted in Fig. 9(b). Initially, the peak radial flux (~1 MW/cm^2) is much larger than the peak axial flux (~26 kW/cm^2). After ~1 cm of propagation, the radial and the axial flux are both of order ~1 kW/cm^2. Note that a quasiequilibrium state is attained after ~0.3 cm of propagation in which the laser intensity and plasma density change slowly relative to the initial phase of propagation in which the air was close to fully ionized.

Figure 10 plots the corresponding spatial distributions of laser intensity, and Poynting flux in the quasiequilibrium configuration at a propagation distance $z=0.8$ cm. The radius of the plasma filament in these plots is ~0.5 mm. Due to the high electron collision frequency, there is little axial flux in the region $r<0.25$ mm, while the radial flux is seen to be strongly damped behind the laser pulse.

B. EMP Generation on the Surface of a Dielectric

In this section, we simulate the EMP generation from the interaction of a laser pulse with a dielectric surface. The simulation is set up with air in the region $z<0$ and a dielectric in the region $z>0$. The initial laser pulse at $t=0$ is situated just outside the dielectric and has a field envelope that is Gaussian in the transverse direction with a spot size $R_o=0.1$ mm. The longitudinal laser field profile is given by Eq. (25) with $\tau_L=200$ fsec. The laser pulse has wavelength $\lambda_o=0.8$ μm($\hbar\,\omega_o=1.54$ eV) and peak intensity $I_L=10^{13}$ W/cm^2. The dielectric is characterized by $n_{no}=6\times10^{22}$ cm^{-3}, $n_o=3$, $n_K=7\times10^{-15}$ cm^2/W, $U_{ion}=3$ eV, $\ell=2$, and $I_{MP}=5\times10^{14}$ W/cm^2. The WKB solution, i.e., Eq. (60), is evaluated numerically to obtain evolution of the laser pulse within the dielectric, and Eq. (50) is solved to determine the EMP generation.

Figure 11 plots contours of the laser intensity I_L and EMP intensity $I_{EMP}=(I_r^2+I_z^2)^{1/2}$ in the (z,r) plane at various times during the simulation. Figure 11(a) shows the laser intensity contours before the interaction at $t=0$. Figure 11(b) shows the simulation results immediately after the front of the laser pulse enters the dielectric and the initial EMP is generated. The EMP extends radially on the order of the laser spot size and longitudinally ~50 μm into the dielectric. The EMP has a peak intensity of $I_{EMP}\sim30$ MW/cm^2 near the boundary. At this time, a plasma layer of width ~5 μm, radial extent ~100 μm, and peak density $n_e\sim3.5\times10^{21}$ cm$^{-3}(\omega_p\sim3.3\times10^{15}$ sec$^{-1})$ is formed at the boundary. The laser pulse is absorbed within several microns of the boundary.

Figure 11(c) shows the EMP as the trailing end of the laser pulse approaches the boundary. At this instant, the peak EMP intensity is $I_{EMP}\sim7$ MW/cm^2 within the dielectric. Outside the dielectric, an EMP traveling in the negative z direction is observed. Figure 11(d) shows simulation results later in time after the laser pulse has been completely absorbed in the dielectric. There is relatively little EMP flux within the dielectric, most of it has been either reflected or absorbed by the plasma. At this time, the peak plasma density is $n_e\sim9\times10^{21}$ cm^{-3}. Within the dielectric, a pulse of intensity ~300 kW/cm^2 traveling in the positive z direction is observed.

As noted in Sec. III, the interaction of a laser pulse with a dielectric can also lead to the generation of bremsstrahlung radiation. The conversion efficiency for bremsstrahlung is estimated to be on the order of $\sim10^{-4}$, which is significantly higher than the EMP conversion efficiency.

V. SUMMARY

In this paper the generation of EMP by ultrashort laser pulses in air and on dielectric surfaces is analyzed and dis-

cussed. Multiphoton ionization leads to the creation of a plasma filament in the medium. The plasma currents driven by the ponderomotive forces associated with the laser pulse are the source of the EMP. The plasma currents, however, decay rapidly behind the laser pulse due to the large electron collision frequency. For a plasma density of $n_e \sim 10^{16}$ cm^{-3}, the electron collision frequency is $\nu_e \sim 5 \times 10^{12}$ sec^{-1} (for $T_e = 1$ eV), and the duration of the plasma current is $\sim 1/\nu_e \sim 200$ fsec. The duration of the EMP at a fixed axial position is roughly equal to the laser pulse duration plus the plasma decay time, $\sim \tau_L + 1/\nu_e$, which is typically a few hundred femtoseconds. The conversion efficiency from the laser pulse to EMP radiation is found to be extremely small in both air and on dielectric surfaces. Typical conversion efficiencies are on the order of 10^{-9}. The EMP frequency spectrum is broad with a characteristic frequency determined by the laser pulse duration and the electron collision time and not by the local plasma frequency. Our results are fundamentally different from those in Refs. [30,31]. For example, in a steady state propagation regime the EMP is nonradiative and the energy flux is axially directed with no net radial component. We show that in a transient propagation regime radiative flux of EMP energy is possible provided a Cherenkov-like condition is satisfied. Several examples of EMP generation have been simulated and discussed. Our results predict a peak EMP power of ~ 8 W for the parameters of the experiment in Ref. [17], corresponding to an efficiency of $\sim 10^{-9}$ for the radial power flow. In another example, using a high energy laser pulse (0.5 J) we find that the ionization losses of the laser pulse are significant and that the pulse eventually reaches a quasiequilibrium state. Finally, simulations of EMP generation from the interaction of a laser pulse with a dielectric medium show that EMP intensities on the order of MW/cm^2 can be generated. Most of the EMP energy, however, is reflected by the plasma formed at the surface of the dielectric.

[1] A. Braun, G. Korn, X. Liu, D. Du, J. Squier, and G. Mourou, Opt. Lett. **20**, 73 (1995).

[2] E. T. Nibbering, P. F. Curley, G. Grillon, B. S. Prade, M. A. Franco, F. Salin, and A. Mysyrowicz, Opt. Lett. **21**, 62 (1996).

[3] O. G. Kosareva, V. P. Kandidov, A. Brodeur, C. Y. Chien, and S. L. Chin, Opt. Lett. **22**, 1332 (1997).

[4] L. Wöste, C. Wedekind, H. Wille, P. Rairoux, B. Stein, S. Nikolov, Ch. Werner, St. Niedermeier, F. Ronneberger, H. Schillinger, and R. Sauerbrey, Laser Optoelektron. **29**, 51 (1997); J. Kasparian, M. Rodriguez, G. Méjean, J. Yu, E. Salmon, H. Wille, R. Bourayou, S. Frey, Y.-B. André, A. Mysyrowicz, R. Sauerbrey, J.-P. Wolf, and L. Wöste, Science **301**, 61 (2003).

[5] B. La Fontaine, F. Vidal, Z. Jiang, C. Y. Chien, D. Comtois, A. Desparois, T. W. Johnston, J.-C. Kieffer, H. Pepin, and H. P. Mercure, Phys. Plasmas **6**, 1615 (1999).

[6] S. Tzortzakis, L. Berge, A Couairon, M. Franco, B. Prade, and A. Mysyrowicz, Phys. Rev. Lett. **86**, 5470 (2001); A. Couairon, S. Tzortzakis, L. Berge, M. Franco, B. Prade, and A. Mysyrowicz, J. Opt. Soc. Am. B **19**, 1117 (2002).

[7] C. Y. Chien, B. La Fontaine, A. Desparois, Z. Jiang, T. W. Johnston, J.-C. Kieffer, H. Pepin, F. Vidal, and H. P. Mercure, Opt. Lett. **25**, 578 (2000).

[8] J. Kasparian, R. Sauerbrey, D. Mondelain, S. Niedermeier, J. Yu, J.-P. Wolf, Y.-B. Andre, M. Franco, B. Prade, S. Tzortzakis, A. Mysyrowicz, M. Rodriguez, H. Wille, and L. Wöste, Opt. Lett. **25**, 1397 (2000).

[9] J. Yu, D. Mondelain, G. Ange, R. Volk, S. Niedermeier, J. P. Wolf, J. Kasparian, and R. Sauerbrey, Opt. Lett. **26**, 533 (2001).

[10] X. M. Zhao, J.-C. Diels, C. Y. Wang, and J. M. Elizondo, IEEE J. Quantum Electron. **31**, 599 (1995).

[11] H. Schillinger and R. Sauerbrey, Appl. Phys. B: Lasers Opt. **B68**, 753 (1999).

[12] S. Tzortzakis, M. A. Franco, Y.-B. Andre, A. Chiron, B. Lamouroux, B. S. Prade, and A. Mysyrowicz, Phys. Rev. E **60**, R3505 (1999).

[13] D. Comtois, C. Y. Chien, A. Desparois, F. Genin, G. Jarry, T. W. Johnston, J.-C. Kieffer, B. La Fontaine, F. Martin, R. Mawassi, H. Pepin, F. A. M. Rizk, F. Vidal, P. Couture, H. P. Mercure, C. Potvin, A. Bondiou-Clergerie, and I. Gallimberti, Appl. Phys. Lett. **76**, 819 (2000).

[14] H. D. Ladouceur, A. P. Baronavski, D. Lohrmann, P. W. Grounds, and P. G. Girardi, Opt. Commun. **189**, 107 (2001).

[15] A. Ting, D. Gordon, D. Kaganovich, E. Briscoe, C. Manka, J. Peñano, P. Sprangle, B. Hafizi, and R. Hubbard, J. Directed Energy **2**, 131 (2004).

[16] A. Proulx, A. Talebpour, S. Petit, and S. L. Chin, Opt. Commun. **174**, 305 (2000).

[17] S. Tzortzakis, G. Méchain, G. Patalano, Y. B. André, B. Prade, M. Franco, A. Mysyrowicz, J. M. Munier, M. Gheudin, G. Beaudin, and P. Encrenaz, Opt. Lett. **27**, 1944 (2002).

[18] J. Kasparian, M. Rodriguez, G. Mejean, J. Yu, E. Salmon, H. Wille, R. Bourayou, S. Frey, Y.-B. Andre, A. Mysyrowicz, R. Sauerbrey, J.-P. Wolfe, and L. Woste, Science **301**, 61 (2003).

[19] G. Kozlov and A. Volkov, in *Millimeter and Submillimeter Wave spectroscopy of Solids*, edited by G. Grüner (Springer-Verlag, Berlin, 1998), Chap. 3, p. 52.

[20] T. Idehara *et al.*, IEEE Trans. Plasma Sci. **27**, 340 (1999).

[21] G. L. Carr *et al.*, Phys. Med. Biol. **47**, 3761 (2002).

[22] Z. Jiang and X. C. Zhang, in *Sensing with Terahertz Radiation*, edited by D. Mittleman (Springer-Verlag, Berlin, 2003) p. 155.

[23] M. C. Nuss and J. Orenstein, in *Millimeter and Submillimeter Wave spectroscopy of Solids* (Ref. [19]), Chap. 2, p. 7.

[24] K. Kawase, H. Minamide, K. Imai, J. Shikata, and H. Ito, Appl. Phys. Lett. **80**, 195 (2002).

[25] E. Bründermann, D. R. Chamberlin, and E. E. Haller, Appl. Phys. Lett. **76**, 2991 (2000).

[26] E. R. Mueller, in *Encyclopedia of Electrical and Electronic Engineering*, edited by J. G. Webster (Wiley, New York, 1999), Vol. 20, p. 597.

[27] C. H. Lai *et al.*, Phys. Rev. Lett. **77**, 4764 (1996); D. Hashimshony *et al.*, *ibid.* **86**, 2806 (2001).

[28] N. Yugami, T. Higashiguchi, H. Gao, S. Sakai, K. Takahashi, H. Ito, Y. Nishida, and T. Katsouleas, Phys. Rev. Lett. **89**, 065003 (2002).

[29] P. Sprangle, E. Esarey, A. Ting, and G. Joyce, Appl. Phys. Lett. **53**, 2146 (1988); P. Sprangle, B. Hafizi, J. R. Peñano, R. F. Hubbard, A. Ting, A. Zigler, and T. M. Antonsen, Phys. Rev. Lett. **85**, 5110 (2000); P. Sprangle, B. Hafizi, J. R. Peñano, R. F. Hubbard, A. Ting, C. I. Moore, D. F. Gordon, A. Zigler, D. Kaganovich, and T. M. Antonsen, Phys. Rev. E **63**, 056405 (2001).

[30] C. C. Cheng, E. M. Wright, and J. V. Moloney, Phys. Rev. Lett. **87**, 213001 (2001).

[31] C. C. Cheng, E. M. Wright, and J. V. Moloney, Phys. Rev. Lett. **89**, 139302 (2002).

[32] G. Shvets, I. Kaganovich, and E. Startsev, Phys. Rev. Lett. **89**, 139301 (2002); V. T. Tikhonchuk, *ibid.* **89**, 209301 (2002).

[33] J. R. Peñano, P. Sprangle, P. Serafim, B. Hafizi, and A. Ting, Phys. Rev. E **68**, 056502 (2003);

[34] P. Sprangle, E. Esarey, and B. Hafizi, Phys. Rev. Lett. **79**, 1046 (1997); Phys. Rev. E **56**, 5894 (1997); P. Sprangle, B.

Hafizi, and J. R. Peñano, *ibid.* **61**, 4381 (2000).

[35] *NRL Plasma Formulary*, edited by J. D. Huba, Naval Research Laboratory Publication NRL/PU/6790-98-358 (U.S. GPO, Washington, D.C., 1998).

[36] P. Sprangle, J. R. Peñano, and B. Hafizi, Phys. Rev. E **66**, 046418 (2002).

[37] L. V. Keldysh, Zh. Eksp. Teor. Fiz. **47**, 1945 (1964) [Sov. Phys. JETP **20**, 1307 (1965)].

[38] B. La Fontaine, F. Vidal, Z. Jiang, C. Y. Chien, D. Comtois, A. Desparois, T. W. Johnston, J.-C. Kieffer, H. Pepin, and H. P. Mercure, Phys. Plasmas **6**, 1615 (1999).

[39] A. W. Ali, Naval Research Laboratory Memorandum Report No. 4619 1981 (unpublished).

[40] P. Sprangle, J. R. Peñano, A. Ting, B. Hafizi, and D. F. Gordon, J. Directed Energy **1**, 73 (2003).

[41] R. W. Boyd, *Nonlinear Optics* (Academic, San Diego, 1992).

[42] P. Sprangle, A. Ting, and C. M. Tang, Phys. Rev. A **36**, 2773 (1987).

[43] D. H. Auston, Appl. Phys. Lett. **43**, 713 (1983).

[44] S. C. Howells and L. A. Schlie, Appl. Phys. Lett. **67**, 3688 (1995).

[45] H. M. Milchberg and R. R. Freeman, J. Opt. Soc. Am. B **6**, 1351 (1989).

[46] C. H. Lee, *Picosecond Optoelectronic Devices* (Academic, Orlando, 1984).